ABSTRACT

Title of Dissertation: COMSOLOGICAL PHASE TRANSITION OF COMPOSITE HIGGS CONFINEMENT

Majid Ekhtetrachian
Doctor of Philosophy, 2021

Dissertation Directed by: Kaustubh Agashe
Department of Physics

We study the cosmological confinement-deconfinement phase transition (PT) of nearly conformal, strongly coupled large N field theories, applicable to composite Higgs models. We find that despite strong coupling, aspects of the PT can be analyzed when the confinement is predominantly spontaneous. In this scenario, the leading contribution to the transition rate can be computed within effective field theory of dilaton– the pseudo Nambu-Goldstone boson associated with the spontaneous breaking of conformal symmetry. We then show how the holographic dual formulation in terms of 5D warped compactifications allows for qualitative understanding of the missing pieces of the earlier described 4D picture and a quantitative improvement of the calculations. In this description the PT is from a high-temperature black-brane phase to the low-temperature Randall-Sundrum I phase, and the transition proceeds by percolation of bubbles of IR-brane nucleating from the black-brane horizon. We show that the bubble configuration interpolating between the two phases can be smooth enough to be described within 5D effective field theory. We find that

cosmological PT in the minimal models can complete only after a large period of supercooling, potentially resulting in excessive dilution of primordial matter abundances. We then show how generic modifications of the minimal models can result in a much faster completion of the PT. We also study the stochastic gravitational wave background produced by the violent bubble dynamics and discuss the implications of the PT for baryogenesis.

COMSOLOGICAL PHASE TRANSITION OF COMPOSITE HIGGS CONFINEMENT

by

Majid Ekhterachian

Dissertation submitted to the Faculty of the Graduate School of the
University of Maryland, College Park in partial fulfillment
of the requirements for the degree of
Doctor of Philosophy
2021

Advisory Committee:
Professor Kaustubh Agashe, Chair/Advisor
Professor Zackaria Chacko
Professor Thomas Cohen
Professor Raman Sundrum
Professor Richard Wentworth

Preface

This main part of the work for this thesis is done in collaboration with other people. The thesis is mostly based on *JHEP 05 (2020) 086* [1] and *JHEP 02 (2021) 051* [2], both of which are co-authored with Kaustubh Agashe, Peizhi Du, Soubhik Kumar and Raman Sundrum.

Dedication

To my parents Fariba Sha'bani and Mohsen Ekhterachian.

Acknowledgments

I owe my gratitude to all those who have made this thesis possible and because of whom my experience in graduate school has become one to remember forever.

First, I would like to thank my advisor, Professor Kaustubh Agashe for giving me the opportunity to work with him on several interesting projects. The experience of working with him has helped me grow in both technical and professional aspects. I appreciate his invaluable support at every stage of my graduate school experience, and his patience in addressing all my concerns and questions.

I would also like to thank Professor Raman Sundrum. I have been very fortunate for having the opportunity to work with him on several projects, to get his advice and to discuss various ideas with him regularly, and to be able to take three courses with him through which I learned a lot about quantum field theory and particle physics. These all have enriched my experience in graduate school.

Thanks are due to Professor Zackaria Chacko, Professor Thomas Cohen and Professor Richard Wentworth for agreeing to be on my dissertation committee and for spending their precious time reviewing the manuscript of the dissertation.

I would also like to thank the people who I have had the chance to collaborate with on different projects during graduate school. They include Arushi Bodas, Daniel Carney, Kaustubh Deshpande, Peizhi Du, Reza Ebadi, Chee Sheng

Fong, Sugnwoo Hong, Anson Hook, Doojin Kim, Soubhik Kumar, Zhen Liu, Deepak Sathyan, Yuhsin Tsai, and Luca Vecchi.

Many other fellow graduate students and post-docs have had important influences on my thinking and interactions with them has been very fruitful. I would like to thank Stefano Antonini, Batoul Banihashemi, Jack Collins, Saurav Das, Abhish Dev, David Curtin, Michael Geller, Gustavo Marques Tavares, and Rashmish Mishra.

I appreciate my parents for their unlimited support and encouragement. I would also like to especially thank Zahra for her invaluable friendship and support.

I would also like to acknowledge help and financial support from Maryland Center for Fundamental Physics (MCFP) and National Science Foundation (NSF).

It is not possible to remember all, and I apologize to those that I have unintentionally left out.

Table of Contents

List of Tables

List of Figures

List of Abbreviations

4(5)D	Four (five) dimensional
AdS	Anti-de Sitter
AdS-S	Anti-de Sitter-Schwarzschild
BSM	Beyond the standard model
CFT	Conformal field theory
d.o.f	degrees of freedom
EFT	Effective field theory
EoM	equation of motion
eV, keV, MeV, GeV, TeV	Electro-volt, kilo-, mega-, giga-,tera- electron-volt
EW	Electroweak
FP	Fixed point
GW	Gravitational Waves
IR	Infrared
KK	Kaluza-Klein
LHC	Large Hadron Collider
LISA	Laser Interferometer Space Antenna
pNGB	Pseudo-Nambu-Goldstone boson
PT	Phase transition
QCD	Quantum Chromodynamics
RG	Renormalization group
RGE	Renormalization group equation
RS	Randall-Sundrum
SM	Standard model (of particle physics)
UV	Ultraviolet
VEV	Vacuum expectation value

Chapter 1: Introduction

With the discovery of the Higgs boson at the Large Hadron Collider (LHC) [4, 5], all of the particles in standard model (SM) have been observed. The SM has been extremely successful in predicting and explaining a variety of experimental results and passing different stress-tests. However it can not be the final theory of fundamental physics. To have a complete description of gravity, the SM needs to be extended or modified. Moreover, the SM does not account for the dark matter, does not give mass to the neutrinos, and cannot explain the observed matter-antimatter asymmetry of the universe.

The SM is best viewed as an effective field theory (EFT), valid up to some energy scale $\Lambda_{\mathrm{N}P}$. As an EFT, given the field content of the theory and their (gauge) quantum numbers, one writes a Lagrangian with all allowed terms, which are gauge and Lorentz invariant operators made out of the constituent fields with arbitrary coefficients/couplings. There are infinite such terms that can be written down, but for processes happening at a energy scale E smaller than the cutoff $\Lambda_{\mathrm{N}P}$, the contribution of higher-dimensional operators with mass-dimension $d_i > 4$ are suppressed by $\left(\frac{E}{\Lambda_{\mathrm{N}P}}\right)^{d_i-4}$. Hence, at low energies and given a specific precision, one can limit the operators considered in the EFT to the ones below some dimension.

In this view, part of the success of the SM can be understood in terms of the accidental symmetries that emerge at low energies: assuming that Λ_{NP} is large and hence keeping only operators of dimension $d \leq 4$ [1] in the Lagrangian, one gets only a limited set of interactions which respect global (exact and approximate) symmetries that were not imposed. These symmetries include the global symmetries that result in baryon and lepton family number conservations. This for example explains why the proton is expected to have a long lifetime as its decay is forbidden as long as baryon number is conserved. Proton decay has not been observed yet, and its non-observation can be explained by taking the scale suppressing the corresponding higher dimensional operators to be larger than $\mathcal{O}(10^{15})$ GeV. It is also worth noting that the small observed neutrino masses and mixings can be implemented in this SM EFT by including the operator with lowest dimension beyond the renormalizable Lagrangian (i.e. with $d = 5$), suppressed by a scale of $\mathcal{O}(10^{14})$ GeV. Moreover, lack of deviation in various CP and flavor violating processes from the (renormalizable) SM predictions suggest a cutoff scale Λ_{NP} much larger than the TeV scale for the SM as an EFT.

This of course does not mean that all higher dimensional operators necessarily have to be suppressed by such a high scale, as is possible that new physics may show up at lower energies, while still having accidental symmetries similar to those of the SM. However, let us for now assume that this is the case, i.e. that the SM is an EFT with a cutoff Λ_{NP} much above the TeV scale. In this picture, one then

[1] Usually "the Standard Model" refers to the renormalizable Lagrangian made up of only these terms.

expects, by dimensional analysis, that coefficient of relevant operators are also set by the same scale. The unique dimension 2 operator in the SM is the mass term for the Higgs boson, $m_H^2 H^\dagger H$, which we may write as $c_2 \Lambda_{\rm NP}^2 H^\dagger H$.

We can naturally expect that c_2 is of order one, which makes m_H^2 much larger than the square of the observed Higgs mass. One may ask what if somehow the UV physics at $\Lambda_{\rm NP}$ gives a very small c_2? Of course in that case one should look for an explanation of why c_2 is so small, but if possible, this may postpone this question to much higher scales. So let's assume for now that after integrating out the heavy physics, we get a tiny c_2 and see if it solves the problem. To obtain the physical Higgs mass and/or the parameters relevant for the electroweak symmetry breaking, it is more convenient to use the renormalization group equations (RGE) and run down to the renormalization group (RG) scale near the weak scale. This running gives a contribution to the above dimension-two operator dominated by the effect of the top loop, which would be $\delta m_H^2 \sim \frac{3y_t^2}{16\pi^2}\Lambda_{\rm NP}^2$, where y_t is the top Yukawa coupling. So to obtain the observed Higgs mass, there has to be a very precise cancellation between $c_2\Lambda_{\rm NP}^2$ at the UV cutoff of the EFT and the contributions between that scale all the way down to the electroweak scale. This is the hierarchy problem.

To solve the hierarchy problem, it is clear from the discussion above that the new physics should be introduced at a scale not very far from the electroweak scale. Moreover, the new physics should be such that it does not reintroduce the problem. This is possible if either the Higgs mass term and similar dimension 2 operators are absent in the new model, or that they are protected from large quantum corrections from the higher energy scales. The two main known class of solutions to the hierarchy

problem indeed use these two options. First class of these solutions invoke a new spacetime symmetry, i.e. supersymmetry, which protects the Higgs mass from large UV corrections (see [6] for review and references). In the second class of solutions, known as the composite Higgs models (see references [7,8] for a review), the Higgs is not an elementary particle, and above its compositeness scale there is no Higgs mass term (or similar scalar mass terms). The compositeness scale is generated analogous to what happens in quantum chromodynamics (QCD).

In fact, QCD gives rise to relatively light composite scalars, called pions. The low energy EFT of the pions, known as the chiral Lagrangian, does however have a cutoff not very far from the pion masses as expected from the above naturalness discussion. Also the description above that cutoff, which is the QCD itself, does not contain any scalars and so does not have a hierarchy problem. The QCD scale Λ_{QCD} is much smaller than the cutoff scale for the QCD or the SM, which for now let's take to be $\Lambda_{\rm UV}$. This is however generated from the running of the dimensionless QCD gauge coupling g_s, $\ln \frac{\Lambda_{\rm UV}}{\Lambda_{QCD}} \sim \frac{1}{g^2_{s,\rm UV}}$, where $g_{s,\rm UV}$ is the QCD running gauge coupling at the scale $\Lambda_{\rm UV}$. So the large hierarchy between $\Lambda_{\rm UV}$ and Λ_{QCD} is generated by exponentiation of a small, but not too small, dimensionless $g_{s,\rm UV}$. This generation of a scale from a dimensionless parameter is called dimensional transmutation. As we will see in chapter 2, the compositeness scale for the composite Higgs models is generated in an analogous fashion.

In composite Higgs theories, Higgs boson is a tightly confined composite made of more fundamental constituents. These theories, in addition to addressing the hierarchy problem mentioned, can explain the hierarchical flavor structure of the SM.

Due the strong coupling dynamics, theoretical analysis of these models is challenging. Composite Higgs flavor-physics typically requires strong coupling over a large hierarchy of scales, such as occurs in the domain of an approximate fixed point (FP) of the renormalization group (RG), and plausibly a large-N(color) structure (see reference [9] for a review of large N). Greater theoretical control of the strong dynamics is then possible if the large-N approximate FP conformal field theory (CFT) has a useful Anti-de Sitter (AdS)/CFT dual description [10–12]. Indeed, most of the realistic model building has been done in such a holographic dual higher-dimensional Randall-Sundrum (RS) warped spacetime [13–16] (see [17, 18] for reviews).

In composite Higgs theories, at high enough temperatures, the Higgs boson and other composites of the new strong dynamics are dissolved into their constituents. In this thesis, we study this confinement-deconfinement phase transition (PT). This PT is particularly important in studying the cosmological history of the universe in these theories. In the early universe the temperature can be high enough for it to be in deconfined phase. Then one important question is wether the universe would ever get out of this phase. This is essential for these theories to having a consistent cosmological history, since if they describe our universe, we should now be living in the confined phase. Also even if the phase transition completes but only after a long period of supercooling, it will have important consequences for generation of the baryon asymmetry and dark matter, since this period can result in significant dilution of matter abundances.

More generally, first order phase transitions can play an important role in cosmological evolution through dramatic rearrangements of particle physics degrees of

freedom (d.o.f). As out-of-equilibrium processes, such PTs can create new matter asymmetries, or drastically alter pre-existing ones. They also can provide a spectacular source for stochastic gravitational waves (GW) [19–22] (see reference [23] for a review). While the Standard Model Higgs boson does not give rise to a first order electroweak (EW) PT (see reference [24] for a review), this PT can be first order in many beyond-SM (BSM) extensions. Further, BSM extensions may give rise to other PTs, roughly connected to the EW scale by the naturalness principle. There may then be one or more PTs in the $\sim$ TeV - 100 TeV range. If so, we should be able to probe such BSM physics by complementary means, its microphysics at particle collider experiments, and the associated PT in GW detectors [25–29]. Composite Higgs theories which beyond the EW PT itself undergo a fascinating and rich PT (as was mentioned above) are particularly promising in this regard.

Studying the (de)confinement PT of composite Higgs theories, like studying other aspects of them, is difficult because of the strong coupling dynamics. In this work we will approach this problem from two directions. In chapter 3, we use the holographic dual description of these theories which allows for a weakly coupled and geometric description of the PT. But before using that description, in chapter 2, we first focus on another controlled regime, already visible in four dimensional (4D) spacetime without using AdS/CFT. This happens if the breaking of approximate conformal invariance by confinement is primarily *spontaneous*, resulting in a light pseudo Nambu-Goldstone boson (PNGB) "dilaton" field ϕ [30]. The vacuum expectation value (VEV) of the dilaton field $\langle\phi\rangle$ gives the confinement scale which sets the masses of generic composites. This structure was first seen in composite

Higgs theories in the dual RS formulation in terms of the "radion" [13, 14, 31]. In chapter 2 analyze the PT using the 4D dilaton effective field theory [16, 32–37] and reasonable physical expectations, as far as possible. In particular, we study the conditions under which the dilaton dynamics dominates the bubble nucleation rate, which competes with the cosmological expansion rate. The pioneering reference [3] had already argued for dilaton dominance in the RS context, but not completely within higher-dimensional EFT control, and they showed that the PT cannot be prompt in the minimal RS model. References [38–40] showed that the PT could nevertheless complete after a period of supercooling, assuming dilaton dominance (see also [41–45] for further studies of supercooling). Our results will reinforce the earlier work more systematically.

Ultimately, a more complete description and better justification of these expectations can be achieved by modeling the deconfined phase, outside the regime of dilaton EFT. This is a task that we will come back to in chapter 3, where we use the dual description. This dual description, as already indicated, requires large N and yields a more tractable semi-classical, but higher-dimensional description of non-perturbative 4D deconfinement in terms of a black brane horizon. The confinement PT then corresponds to bubbles of the RS "IR brane" nucleating and expanding from this horizon [3]. Our 5D analysis further justify and sharpen the dilaton dominance approximation and account for subleading corrections. We will show that a controlled calculation of the bubble nucleation rate, within the 5D EFT, can be done using an ansatz that we introduce which smoothly interpolates between the two phases.

In composite Higgs models (again in the 4D description), the large hierarchy between the Planck and the weak scales is explained by a small deviation of the theory from scale invariance, where the parameter characterizing the small deviation generates the weak scale by dimensional transmutation. In the minimal models, the same small parameter however significantly suppresses the transition rate, forbidding the completion of PT or delaying it until after a large amount of supercooling. For further studies along these lines see refs. [41–45]. Large supercooling would strongly dilute any primordial (dark) matter abundances, produced before the PT, potentially invalidating such primordial production as the dominant source of (dark) matter seen today. We will show that in a scenario where the composite theory runs from the proximity of an ultraviolet (UV) renormalization group fixed point (FP) to that of an infrared (IR) FP, it is possible to have a much faster transition rate, avoiding large primordial matter dilution. In this scenario the small anomalous dimension corresponding to the UV FP generates the large hierarchy, while the anomalous dimension corresponding to the IR FP, which can be much larger, controls the transition rate. We will also present a robust AdS/CFT dual realization of this two FP scenario in an explicit 5D model, where the extrema of a generic potential for the Goldberger-Wise scalar field [31] play the role of the FPs. Refs. [46–51] also explored the possibility of faster PTs within other non-minimal models.

We also study the stochastic gravitational wave background produced by this PT. We will show systematically that, as it was pointed out in ref. [38, 41], the strength of the stochastic gravitational wave signal arising from the PT (specifically from the better understood bubble collisions) is correlated with the degree of super-

cooling (and matter dilution). We quantitatively present this relationship using our 5D results and the variability of supercooling in our two-FP scenario. Of course, the strength of the stochastic gravitational wave signal is critical for being able to detect beyond astrophysical background and detector noise, but the signals can be large enough that even the primordial anisotropies (analogous to those famously seen in the cosmic microwave background) could be observable at future detectors [52]. The gravitational wave detectors have to have sensitivity at frequencies determined by the critical temperature T_c of the PT. In the composite Higgs scenario $T_c \sim \mathcal{O}(\text{TeV})$, corresponding to $\mathcal{O}(\text{mHz})$ detection frequencies, but quite different frequencies and T_c are possible if an analogous PT occurs in a hidden sector [53]. Our results are straightforwardly transferable to such hidden sector PTs.

Rest of the thesis is organized as follows. In chapter 2 , we study the phase transition from the four dimensional view point. We show how using the dilaton EFT, we can obtain the parametrically dominant contribution to the bubble nucleation rate for this phase transition. We also show how by considering generalizations of the minimal model for stabilization of the confinement scale, the transition rate can become much faster. In chapter 3, we revisit the analysis of the PT from the dual five-dimensional view. We show that the part of the bubble configuration that could not be captured within the dilaton EFT, can be described by a smooth geometric description in the 5D EFT. We also show a concrete 5D realization of our 4D two fixed-point scenario that results in faster phase transition. In chapter 4, we study the stochastic gravitational wave background produced by the phase transition. We then present our conclusions in chapter 5, and point to possible future

directions.

Chapter 2: The 4D view

In this chapter, we study the confinement-deconfinemet phase transition of composite Higgs models, as was briefly outlined in chapter 1, using their 4D description. These models often need strong coupling over a large range of scales, as it happens near RG fixed points, as well as large number of degrees of freedom. So we will consider the confinement-deconfinement PT of approximately scale invariant, strongly coupled large N field theories. Of course, confinement break scale invariance, but this breaking can be predominantly spontaneous. In that case we may use the EFT of the corresponding pNGB to study the PT. We will identify the regime where the dilaton EFT can give the parametrically leading contribution to the bubble nucleation rate, and then use this"dilaton dominance approximation" to analyze the PT.

We first study the equilibrium aspects of the two phases and the PT in section 2.1. In section 2.2 we apply our analysis to the minimal models we will see that the bubble nucleation rate is very small for temperatures near the critical temperature for the PT. This slow rate may prevent the PT form completing, or result in large amount of supercooling before its completion, and such supercooling may dilute pre-existing matter asymmetries to values below the observed matter-antimatter

asymmetry. We then introduce a two-fixed-point model, in which the transition rate can be significantly enhanced, in section 2.3. Then in section 2.4 we study the supercooled PT for both the minimal models and for ours two-FP scenario.

2.1 Equilibrium description of the two phases

We model the deconfined phase as an approximate CFT, coupled to gravity, with $\mathcal{O}(N^2)$ d.o.f. At a temperature T, its free energy (density) F can be written as [3],

$$F_{\text{deconfined}} = V_0 - CN^2T^4, \tag{2.1}$$

where V_0 is a vacuum energy in the deconfined phase and C is some strong-coupling model-dependent $\mathcal{O}(1)$ constant. At low enough T the theory can spontaneously confine giving rise to massive composite states. One of the light composites will be the PNGB dilaton, as noted above. In addition, there may be an $\mathcal{O}(1)$ number of other light composites, in particular the composite Higgs boson, which are weakly coupled to the dilaton by $1/N$. However, it is the dilaton that will play the central role in determining the bubble nucleation rate, as discussed below. We will therefore neglect the other light composites. Further there may be other light elementary particles. They are very weakly coupled to the dilaton, are present in both phases, and are essentially spectators to the PT.

Below the spontaneous confinement scale, we work in the dilaton EFT. We model the small departure from conformal invariance by $\Delta\mathcal{L} = g\mathcal{O}$, where $\mathcal{O}$ is a nearly-marginal composite operator and where the coupling g runs from the UV,

but stops at the confinement scale, locally given by $\phi(x)$. This is the only way in which conformal invariance is broken within the compositeness dynamics, leading to an effective Lagrangian :

$$\mathcal{L}_{\text{eff}} = \frac{N^2}{16\pi^2}\left((\partial\phi)^2 - \lambda\left(g(\phi)\right)\phi^4\right) - V_0, \tag{2.2}$$

where the explicit breaking is characterized by the "running" quartic coupling $\lambda\left(g(\phi)\right)$. We see that if g did not run, the dilaton coupling would be exactly conformally invariant ϕ^4. The vacuum energies of the two phases are equated by matching at the common limit of the two phases, $T = 0$, $\phi = 0$. This vacuum energy also breaks conformal invariance but is only of gravitational relevance. In this standard large-N "glueball" normalization (reviewed in [9, 54]), the self-coupling is expected to be $\lambda \sim 1$. However, it is certainly possible that λ is somewhat smaller, in which case theoretical control can be gained by expanding in λ, as we will see below.

For a small deformation g, we can expand λ to first order,

$$\lambda(g) = \lambda_0 + \lambda_0' g, \tag{2.3}$$

where $\lambda_0 \equiv \lambda(g=0)$ and $\lambda_0' \equiv \frac{d\lambda}{dg}|_{g=0}$. For $\beta(g) \equiv \frac{dg}{d\ln\mu} \approx \epsilon g$, the scaling dimension of $\mathcal{O}$ is determined to be $4+\epsilon$, and $g(\phi) \approx g_{\text{UV}}\left(\frac{\phi}{\Lambda_{\text{UV}}}\right)^{\epsilon}$, where g_{UV} is the deformation at UV cut-off scale Λ_{UV}. Plugging this and eq. (2.3) into eq. (2.2), gives us the explicit form for the leading dilaton potential from which we derive the confinement

scale,

$$\langle\phi\rangle = \Lambda_{\rm UV}\left(-\frac{1}{1+\epsilon/4}\frac{\lambda_0}{\lambda_0' g_{\rm UV}}\right)^{\frac{1}{\epsilon}}. \tag{2.4}$$

We note that an exponentially large hierarchy between $\langle\phi\rangle$ and $\Lambda_{\rm UV}$ can be obtained if ϵ is small, given just a mild hierarchy between λ_0 and $\lambda_0' g_{\rm UV}$ [16]. This is dual to the minimal 5D Goldberger-Wise mechanism [31]. It is convenient to express the potential in terms of $\langle\phi\rangle$,

$$V_{\rm eff} = \frac{N^2}{16\pi^2}\lambda_0\phi^4\left(1-\frac{1}{1+\epsilon/4}\left(\frac{\phi}{\langle\phi\rangle}\right)^{\epsilon}\right)+V_0. \tag{2.5}$$

We choose V_0 to ensure the (almost) vanishing cosmological constant (CC) today, i.e. we impose $V_{\rm eff}(\langle\phi\rangle)=0$. Note that, vacuum stability implies $\epsilon\lambda_0<0$.

Assuming a low critical temperature for the PT, $T_c \ll \langle\phi\rangle$, we can solve for it by equating the free energies of the two phases:

$$\begin{aligned} F_{\rm deconfined}(T_c) = F_{\rm confined}(T_c) &\underset{T_c\ll\langle\phi\rangle}{\approx} V_{\rm eff}(\langle\phi\rangle) \\ \Rightarrow \frac{T_c}{\langle\phi\rangle} &= \left(\frac{-\epsilon\lambda_0}{16\pi^2 C(4+\epsilon)}\right)^{1/4} + \mathcal{O}\left(\frac{1}{N^2}\right). \end{aligned} \tag{2.6}$$

We see that T_c is self-consistently small for small ϵ and/or small λ_0. Therefore the confining phase is within dilaton EFT control. Since the coupling $g(\phi)$ blows up in the IR for $\epsilon<0$, making the bounce calculation unreliable, we will consider $\epsilon>0, \lambda_0<0$ in the minimal set-up. With this choice, approximate conformal invariance only improves in the IR, so that the deconfined phase is expected to exist at arbitrarily small T, including at T_c. This expectation is borne out in the dual

RS analysis [3]. The simultaneously allowed phases at T_c indicate a first-order PT. It follows from eq. (2.6) that $V_0 = CN^2T_c^4$ for vanishing CC today.

A cosmological PT completes for sufficiently large bubble nucleation rate per unit volume, $\Gamma \geq H^4$, where H is the Hubble scale. For $T < T_c$, H asymptotes to a constant, driven by vacuum energy, $H^2 \approx \frac{8\pi}{3} G_N V_0 \sim \frac{CN^2T_c^4}{3M_{\rm Pl}^2}$. Here, G_N and $M_{\rm Pl}$ are respectively Newton's constant and the reduced Planck scale, $M_{\rm Pl} = 2.4 \times 10^{18}$ GeV. Semi-classically the finite temperature bubble nucleation rate Γ, is computed in terms of the Euclidean bounce action $S_{\rm b}$ with time periodicity $1/T$ as,

$$\Gamma \sim T^4 e^{-S_{\rm b}} \underset{\text{completion}}{\geq} H^4. \tag{2.7}$$

Thus for the PT to complete, $S_{\rm b} < 4 \ln\left(\frac{M_{\rm Pl}}{T_c}\right) \sim 140$ for $T_c \sim$ TeV. For small λ, as we would expect, and will show in appendix A, the dominant finite-temperature bounce solutions are $O(3)$ symmetric (and Euclidean time independent).

2.2 Phase transition in the thin-wall regime

Let us first compute Γ in the thin-wall approximation, for prompt PT, $T \approx T_c$. In this approximation quite generally [55, 56]

$$S_{\rm b} = \frac{S_3}{T} = \frac{16\pi}{3} \frac{S_1^3}{(\Delta F)^2 T}, \tag{2.8}$$

where ΔF is the free energy difference between the two phases and S_1 is the surface tension of the bubble wall. The bubble has to interpolate between the de-confined

and the confined phases, see FIG. 2.1. This interpolation consists of two regions, (i) the lowering of the dynamical confinement scale from $\langle\phi\rangle$ down to $\sim T_c \ll \langle\phi\rangle$, followed by (ii) the rearrangement of all d.o.f from confined into deconfined at $\lesssim T_c$ scales. The first region is described purely within the dilaton EFT. To see this note that the dilaton bounce solutions have $|\nabla\phi| \sim \sqrt{V_{\rm eff}}$ which implies $|\nabla\phi|/\phi^2 \sim \sqrt{|\lambda(g)|} \ll 1$ for small λ_0. Thus for $\phi > T_c$, gradients and T are smaller than the local mass gap ϕ, and do not excite the heavier composite d.o.f. In this dilaton dominance approximation we find

$$S_1^{(\rm i)} \approx \frac{N}{2\pi}\int_{\sim T_c}^{\langle\phi\rangle} d\phi\sqrt{V_{\rm eff}} \approx 0.6\Big(\frac{C^3}{\epsilon|\lambda_0|}\Big)^{1/4} N^2 T_c^3. \tag{2.9}$$

We see this is enhanced by small ϵ and λ_0 in T_c units because ϕ is getting large in these units over the bounce trajectory as seen from eq. (2.6). We are therefore insensitive to the lower limit of integration which we can approximate as vanishing. In region (ii), $\phi/T_c \sim \mathcal{O}(1)$ so that we do not expect enhancement by small ϵ or λ_0. Therefore we have dilaton dominance, $S_1 \approx S_1^{(\rm i)}$,

$$\frac{S_3}{T} \approx 3.6\left(\frac{1}{|\lambda_0|\epsilon}\right)^{\frac{3}{4}} C^{\frac{1}{4}} N^2 \frac{T_c/T}{\big(1-(T/T_c)^4\big)^2}. \tag{2.10}$$

Let us apply the above result to the case of a PT at very roughly TeV scale in the minimal scenario in which ϵ accounts for the Planck-TeV hierarchy, $\epsilon \approx 1/25$. But we see from eq. (2.10) that a prompt PT cannot occur within theoretical control, even for $|\lambda_0| = 1/2$, $\frac{T_c^4 - T^4}{T_c^4} = 1/2$ and $N > 1$! To allow the PT to happen

for larger values of N, we need larger values of ϵ while still somehow generating a large hierarchy. We now describe a simple scenario which achieves that.

2.3 A two-FP RG evolution

Earlier, to obtain eq. (2.5) we approximated $\beta(g) \approx \epsilon g$ for near-FP behavior. However, it is possible that the running flows to this vicinity from a different UV FP at g_*. We then have two important critical exponents:

$$\beta(g) = \begin{cases} \epsilon'(g_* - g) & \text{for } g \text{ near } g_* \\ \\ \epsilon g & \text{for } g \text{ small.} \end{cases} \tag{2.11}$$

The transition between the two regimes happens around some intermediate coupling, $g \sim g_{\rm int}$ at a scale $\Lambda_{\rm int} \sim \Lambda_{\rm UV} \left(\frac{g_* - g_{\rm UV}}{g_* - g_{\rm int}}\right)^{1/\epsilon'}$. The confinement scale is now generated from $\Lambda_{\rm int}$ analogously to eq. (2.4) but with replacements $\Lambda_{\rm UV} \to \Lambda_{\rm int}$ and $g_0 \to g_{\rm int}$,

$$\langle\phi\rangle \sim \left(\frac{g_* - g_{\rm UV}}{g_* - g_{\rm int}}\right)^{1/\epsilon'} \left(-\frac{\lambda_0}{(1+\epsilon/4)\lambda_0' g_{\rm int}}\right)^{1/\epsilon} \Lambda_{\rm UV}. \tag{2.12}$$

We see that we can now have a larger ϵ controlling the PT dynamics while still having a large Planck-TeV hierarchy given by small ϵ' (for a related idea see [45]). Eq. (2.5) implies that the dilaton mass$^2 \propto \epsilon$, and hence a larger ϵ implies a heavier dilaton relative to the confinement scale $\langle\phi\rangle$, relevant for collider searches. The above two-FP structure of RG running can be simply modeled with a suitable 5D scalar potential in the dual RS formulation as we will show in chapter 3. By contrast,

the standard Goldberger-Wise 5D scalar [31] with only a mass term in the RS "bulk" is dual to the minimal scenario discussed above.

For a benchmark set of parameters $\epsilon = 0.5, |\lambda_0| = 0.5, C = 1, \frac{T_c^4 - T^4}{T_c^4} = 1/2$, the bounce action can be obtained using eq. (2.10), with eq. (2.7) showing that the PT can complete promptly for $N \approx 2$. This is marginally in theoretical control. If we are outside the regime/parameters for prompt PT, the universe remains and cools in the deconfined phase, and inflates due to the constant term in eq. (2.1). Ultimately, the PT may complete in a supercooled regime, $T \ll T_c$. We now turn to this analysis.

2.4 Phase transition in the supercooled regime

For $T \ll T_c$, by eqs. (2.1) and (2.5) the release point in ϕ drops [47], see FIG. 2.1 . Therefore the bounce only probes the dilaton potential for small ϕ, $V_{\text{eff}} \approx \frac{N^2}{16\pi^2}\lambda_0\phi^4 + V_0$. In this regime we can use a scaling argument for the $O(3)$ symmetric bounce action,

$$\frac{S_3^{(\text{i})}}{T} = \frac{N^2}{4\pi T}\int dr r^2 \left(\left(\frac{d\phi}{dr}\right)^2 + \lambda_0\phi^4 + 16\pi^2 C T^4\right) \tag{2.13}$$

$$= \frac{N^2}{4\pi|\lambda_0|^{\frac{3}{4}}}\int dx x^2 \left(\left(\frac{d\tilde{\phi}}{dx}\right)^2 - \tilde{\phi}^4 + 16\pi^2 C\right), \tag{2.14}$$

where $\tilde{\phi} = |\lambda_0|^{\frac{1}{4}}\phi/T$ and $x = |\lambda_0|^{\frac{1}{4}} rT$. Thus we see that the $S_3^{(\text{i})}$ is not enhanced by ϵ compared to thin wall eq. (2.10), allowing a larger nucleation rate at low T. The dilaton profile is then given by extremizing this action subject to two boundary

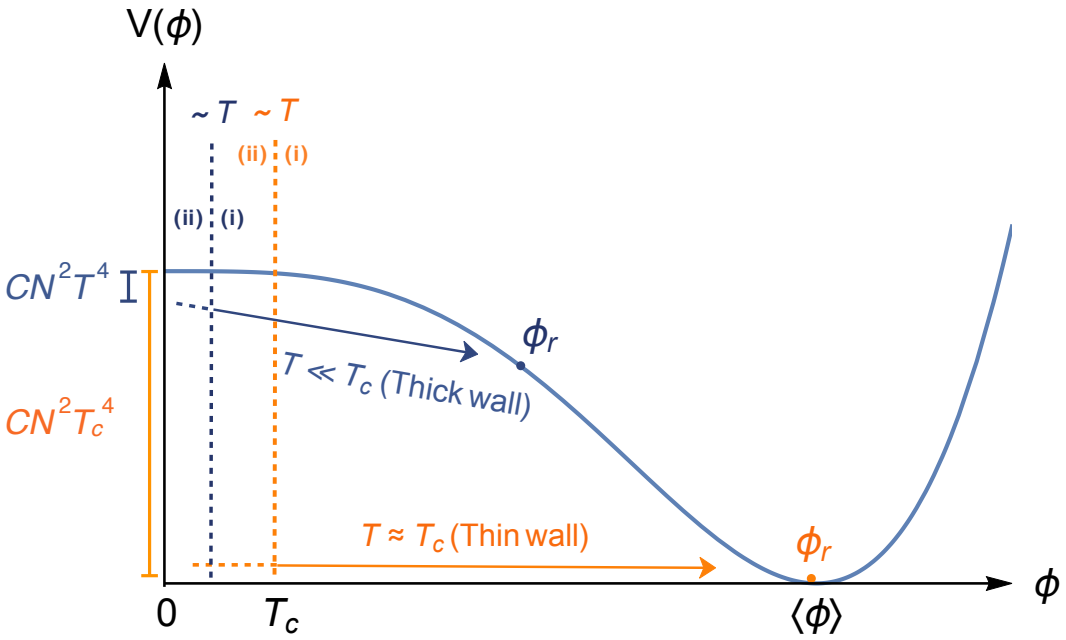

Figure 2.1: The scalar field dynamics of the PT in the prompt (orange) and supercooled (blue) regimes. ϕ_r denotes the release point, characterizing the value of the dilaton field at the center of the bubbles at the moment of their nucleation. The free energy in the deconfined phase is indicated along the vertical axis. The parts of the bounce trajectory to the right/left of the vertical dotted lines correspond to regimes (i)/(ii) in the text giving dominant/sub-dominant contributions to $S_{\rm b}$.

conditions (BC). One is given by $\frac{d\phi}{dr} = \frac{d\tilde{\phi}}{dx} = 0$ at $r = 0$. For the other BC, we first note that part (ii) of the bounce connects to part (i) for $\phi \sim T \ll T_c \ll \langle\phi\rangle$ which we approximate as $\phi \approx 0$ i.e. $\tilde{\phi} \approx 0$. Due to the fact that part (ii) of the bounce is insensitive to small $|\lambda_0| \ll 1$, we will have a λ_0-independent kinetic/gradient energy $(\frac{d\phi}{dr})^2|_{\phi=0} = T^4(\frac{d\tilde{\phi}}{dx})^2|_{\tilde{\phi}=0}$ where $(\frac{d\tilde{\phi}}{dx})^2|_{\tilde{\phi}=0}$ is some $\mathcal{O}(1)$ number which we will fix below. These BCs imply that $\tilde{\phi}(x)$ is independent of λ_0 and therefore the radius of the bubble where $\phi \approx 0$ is $\propto \frac{1}{|\lambda_0|^{1/4}}$. Beyond this radius, the λ_0-independent physics of part (ii) forms a "thin-wall" $\sim (\lambda_0)^0$ around the larger part (i) of the profile. Thus, $S_3^{(\mathrm{ii})}$ is proportional to the area of the bubble $\propto \frac{1}{|\lambda_0|^{1/2}}$. The gradient energy at the matching point $\phi \approx 0$ is then given by the thin-wall approximation $(d\phi/dr)^2 \approx \frac{16\pi^2}{N^2}\Delta F = 16\pi^2 C T^4$. To summarize, $S_3^{(\mathrm{i})} \propto |\lambda_0|^{-3/4}$ while $S_3^{(\mathrm{ii})} \propto |\lambda_0|^{-1/2}$, demonstrating dilaton dominance for $|\lambda_0| \ll 1$. In chapter 3 we will quantify and include the next-to-leading contribution due to region (ii). Having demonstrated dilaton dominance for extreme T, we expect it to hold for all T, in particular, intermediate temperatures. We can then evaluate the bounce action numerically with the boundary condition above. The results of using this prescription and its comparison with the full 5D result will be presented in section 3.5, where we will also further discuss the consequences of supercooling.

In this chapter, we studied the confinement PT of composite Higgs from the strongly coupled 4D description. We showed that dilaton EFT can account for the parametrically dominant contribution to the bounce action, for small ϵ and λ. What we considered so far, however, misses a qualitatively important part of the bounce

configuration which is outside dilaton EFT. In the next chapter we will approach this problem from the dual higher dimensional perspective. The 5D description is weakly coupled and as we will see, gives us a geometric view of the two phases. We will use this description to construct a smooth bounce configuration interploating between the two phases and show that it gives the same leading contribution to the bounce action as we found in this chapter, as well as the subleading correction to it. In the next chapter we will also show a concrete 5D realization of our two-fixed-point scenario that was briefly introduced in this chapter.

Chapter 3: Phase Transition from the Fifth Dimension

Composite Higgs theories often need large number of degrees of freedom $\sim N^2$ of the confined constituents and an approximate conformal symmetry in order to generate the large flavor hierarchies. But this conformal symmetry must break down at the confinement scale. In chapter 2, we focused on the scenario where the breakdown of conformal invariance is *spontaneous*, which we called "spontaneous confinement". There we clarified the parametric regime where the dominant piece of bounce action, controlling the transition rate, can be computed in the confined phase and within the effective field theory of the pseudo Nambu-Goldstone boson of spontaneously broken conformal invariance, namely the dilaton. This parametrically dominant piece, considered in the pioneering ref. [3], accounts only for the approach of the confined phase towards deconfinement, missing the final transition to deconfinement itself where the degrees of freedom are rearranged and the dilaton EFT breaks down. Missing the physics of this final transition to deconfinement means that our final approximate transition rates were useful but still crude.

Further theoretical control is possible when a holographic AdS/CFT dual can be formulated, which is the subject of this chapter. The dual description involves warped compactification of extra dimension(s) as in Randall-Sundrum mod-

els. These theories exhibit a finite temperature black-brane solution as well as a low (or zero) temperature standard RS1 solution. The transition between these two phases is an analog of the well-known Hawking-Page PT of global AdS [57], but in the AdS Poincare patch relevant here, there are significant differences. The transition considered here is dual to the (de)confinement PT mentioned above, where the black brane is dual to the deconfined phase and RS1 is dual to the confined phase. Remarkably, in this dual RS1 formulation, the transition is a non-perturbative 5D quantum gravity process ($\sim e^{-1/G_{N,5D}}$) in which bubbles of IR-brane nucleate from the black-brane horizon, expand and collide, producing an observable stochastic gravitational wave background! And remarkably again, this non-perturbative effect can be captured by semiclassical methods.

This higher dimensional description has been used to study this PT [3, 38, 40, 41, 47, 50, 51, 58, 59], using an ansatz for the bounce configuration describing critical bubbles first introduced in [3]. One might have hoped that the 5D EFT is controlled despite the inevitable breakdown of the 4D dilaton EFT described above. However this particular ansatz is not controlled, even in the 5D EFT, as will be discussed in section 3.2. Quite apart from the detailed extremization of the bounce configuration, 5D EFT control hinges on a qualitative puzzle: how to smoothly interpolate in space-time between the IR-brane and black-brane phases? In this paper, we begin by solving this qualitative problem and show what conditions it places on possible bounce configurations. However, even within this smooth class it is technically challenging to find the extremized bounce configuration that dominates the transition rate. Instead, we introduce a new bounce ansatz within this smooth

controlled class, depicted in figure 3.2, and show that it gives a rigorous and useful lower bound on the transition rate in the thin-wall regime and a very plausible estimate of the rate more generally.

In principle, the smooth class of bounce configurations can be extremized with respect to the 5D action to determine the true transition rate, rather than settling for an ansatz which at best bounds this rate. While we are currently unable to accomplish this feat, it should be noted that in a roughly analogous 6D EFT a domain wall solution between a black-brane phase and an "IR-brane" phase was derived, exploiting a Z_2 symmetry between thermal Euclidean "time" and the sixth dimension [60]. In the thin-wall limit this solution can be recast as a bounce solution for transitioning between the two phases, which we hope to explore in future work.

Both our ansatz and the work related to the prior ansatz of [3] share the correct parametrically dominant dilaton contribution to the bounce. Our improvement is at the level of the parametrically subdominant corrections involving the IR-brane/black-brane juncture. However, these corrections are qualitatively significant as discussed above, and quantitatively significant for realistic choices of parameters.

In chapter 2, we introduced a scenario where the the theory runs from the proximity of a UV FP towards an IR FP. we saw that in this scenario different parameters control the hierarchy and the bubble nucleation rate, which allows for having a much faster transition. In this chapter and in section 3.4 we introduce a concrete 5D model realizing this scenario.

Using our ansatz we estimate the bounce action, which controls the transition rate, for the minimal model and for the two-FP scenario. Comparing this rate with

the dilaton/radion dominance approximation, we identify the subleading corrections and see that in the paramateric regime identified for dilaton dominance the two approaches agree, as expected. Then by comparing the transition rate with the rate of expansion of the universe, we determine if the transition completes, and when it does, we find the temperature at which this happens. We find that staying in the regime where there is a controlled semiclassical approximation to the rate, and for a realistic region of parameter space for which the PT completes, the corrections to the 4D dilaton dominance approximation are quantitatively important, but are captured by our 5D EFT treatment.

3.1 Equilibrium description of the two phases

We start with the general 5D action $S_{5\mathrm{D}}$, which is a sum of S_{GR}, the gravitational action and S_χ, the action of Goldberger-Wise field χ:

$$\begin{aligned} S_{5\mathrm{D}} &= S_{\mathrm{GR}} + S_\chi \\ &= 2M_5^3 \int d^5x\sqrt{-g}\left(R_5 + 12k^2\right) + 4M_5^3 k \int d^4x\sqrt{-\gamma}K - \tau_{\mathrm{bd}} \int d^4x\sqrt{-\gamma} + S_\chi. \end{aligned} \tag{3.1}$$

Here M_5, k are the 5D Planck scale and the AdS curvature scale, respectively. Along with a bulk term that contains the 5D Ricci scalar R_5, S_{GR} also contains a Gibbons-Hawking-York boundary term [61, 62] which make the variation of the bulk action well defined in the presence of boundaries. This boundary term is characterized by $K = g^{\mu\nu}K_{\mu\nu}$, the trace of the extrinsic curvature $K_{\mu\nu}$ of the boundary and,

the induced metric $\gamma_{\mu\nu}$ on the boundary. Lastly, $\tau_{\rm bd}$ denotes the tension on the boundary. In the following we will always work in units where $k = 1$, unless explicitly mentioned.

We first start by neglecting the contribution due to S_χ. In that case the RS metric [13, 14],

$$ds^2 = -\rho^2 dt^2 + \rho^2 \sum_i dx_i^2 + \frac{d\rho^2}{\rho^2}, \tag{3.2}$$

with the extra dimensional coordinate ρ ranging between $\Lambda_{\rm IR} < \rho < \Lambda_{\rm UV}$, represents a solution to $S_{\rm GR}$. Here $\Lambda_{\rm IR(UV)}$ represent the location of the IR (UV) boundary. The tensions on the UV and the IR boundaries are given by $+12M_5^3$ and $-12M_5^3$ respectively. Given a choice of $\Lambda_{\rm UV}$, the scale $\Lambda_{\rm IR}$ corresponds to the VEV of the "radion" field $\phi(x)$ that characterizes the dynamical size of the extra dimension. At this stage $\Lambda_{\rm IR}$ is an arbitrary integration constant corresponding to the fact that ϕ is a flat direction with no potential. In the dual 4D theory, $\Lambda_{\rm IR} \equiv \langle\phi\rangle$ spontaneously breaks the (approximate) conformal symmetry of the composite Higgs dynamics and corresponds to the resulting *spontaneous confinement* scale. The associated Goldstone boson is the dilaton, dual to the radion $\phi(x)$ [15, 16].

To have a predictive theory of $\Lambda_{\rm IR}$ and avoid a massless radion ϕ, the Goldberger-Wise action S_χ needs to be included as a weak perturbation. This leads to a potential for ϕ naturally yielding a hierarchical separation between $\Lambda_{\rm IR}$ and $\Lambda_{\rm UV}$. Over the stabilized hierarchy the RS metric then models the confined phase at $T = 0$. Before discussing the details of the Goldberger-Wise stabilization, let us model the deconfined phase at high T.

At high temperature, $T \gg \Lambda_{\rm IR}$, but $T \ll \Lambda_{\rm UV}$, there is another approximate solution to $S_{\rm GR}$ in eq. (3.1) given by the AdS-Schwarzschild (AdS-S) metric,

$$ds^2 = -\left(\rho^2 - \frac{\rho_h^4}{\rho^2}\right) dt^2 + \rho^2 \sum_i dx_i^2 + \frac{d\rho^2}{\rho^2 - \frac{\rho_h^4}{\rho^2}}. \tag{3.3}$$

This solution is exact for $\Lambda_{\rm UV} = \infty$.

In the metric in eq. (3.3), the surface $\rho = \rho_h$ corresponds to an event horizon and therefore, the coordinate ρ extends between the UV boundary and the horizon, $\rho_h < \rho < \Lambda_{\rm UV}$. Unlike the RS metric in eq. (3.2), the AdS-S metric in eq. (3.3) does not have an IR boundary, which is now instead "hidden" behind the horizon. Given the previous discussion, this absence of the IR boundary indicates an absence of confinement. This lets us model the deconfined 4D theory using the dual AdS-S geometry in eq. (3.3). The temperature of the deconfined plasma is dual to the Hawking temperature corresponding to the horizon,

$$T = \hbar \rho_h / \pi, \tag{3.4}$$

where we have momentarily written the factor of $\hbar$ explicitly for later purposes. Given the absence of the IR boundary, and hence the radion modulus ϕ, the Goldberger-Wise perturbation does not play any significant role unlike the confined phase and is therefore negelcted to a leading approximation.[1]

For finite $\Lambda_{\rm UV}$, there exists an elegant exact solution given in [63]. From the

[1]The non-gravitational scalar action S_χ is not enhanced by a factor of M_5^3/k^3 unlike $S_{\rm GR}$, we will ignore the contribution of S_χ while discussing the deconfined phase.

dual 4D perspective, it corresponds to the 4D deconfined plasma coupled to 4D GR, gravitationally equivalent to a period of FRW radiation dominance. For $\Lambda_{\rm UV} \gg T$, this results in an adiabatic redshifting of T over time. That is to say that even for finite but large $\Lambda_{\rm UV}$, AdS-S metric in eq. (3.3) represents an approximate solution if we take $\rho_h \to \rho_h(t)$, determined by the redshifting (3.4) and the Friedmann equations.

In terms of this quasi-static T, one can calculate the free energy density of the deconfined phase [3],

$$F_{\rm deconfined} = V_0 - 2\pi^4 M_5^3 T^4, \tag{3.5}$$

where V_0 is a possible constant energy density that will be determined in a moment.[2]

To compute the critical temperature corresponding to the PT, we also need to compute the free energy of the RS phase. As mentioned earlier, without Goldberger-Wise S_χ contribution, the radion ϕ is a flat direction. Therefore, the leading contribution to the free energy corresponding to the confined phase at low T comes from the perturbation S_χ in the background of the unperturbed RS metric eq. (3.2),

$$S_\chi = \int d^4x \int_{\Lambda_{\rm IR}}^{\Lambda_{\rm UV}} d\rho \sqrt{-g} \left[-\frac{1}{2}(\partial\chi)^2 - V_\chi(\chi) - \rho\delta(\rho - \Lambda_{\rm UV})\kappa(\chi^2 - v^2)^2 + \rho\delta(\rho - \Lambda_{\rm IR})\alpha\chi \right]. \tag{3.6}$$

[2] In the full model the free energy would also include the contribution of the significant number of (relativistic) non-composite elementary fields of the SM, appearing in 5D as zero modes which are not strongly leaning towards the IR. However, in what follows they are largely "spectators" which will not alter the leading results. We therefore omit them.

A free Goldberger-Wise field, $V_{\rm GW}(\chi) = \frac{1}{2}m^2\chi^2$, with boundary terms above such that they satisfy the boundary conditions for the χ field

$$\chi|_{\rho=\Lambda_{\rm UV}} = v \quad \text{and} \quad \rho\frac{\partial\chi}{\partial\rho}\Big|_{\rho=\Lambda_{\rm IR}} = -\alpha, \tag{3.7}$$

is sufficient to stabilize the geometry [31].[3] The low energy radion effective action (up to two derivative order) is given by eq. (3.1) after promoting $\Lambda_{\rm IR}$ to the 4D radion field $\phi(x)$. In particular, the boundary terms of $S_{\rm GR}$ in eq. (3.1) gives the kinetic term of the radion, and the Goldberger-Wise action in eq. (3.6) gives effective radion potential $V_{\rm rad}$ so that the radion action becomes,

$$\mathcal{S}_{\rm radion} \approx \int d^4x \left(-6M_5^3(\partial\phi)^2 - V_{\rm rad}(\phi)\right). \tag{3.8}$$

The effective radion potential is given by [31],

$$V_{\rm rad}(\phi) = 12M_5^3\lambda\phi^4\left(1 - \frac{1}{1+\epsilon/4}\left(\frac{\phi}{\langle\phi\rangle}\right)^{\epsilon}\right) + V_1, \tag{3.9}$$

where $\lambda = (\tau_{\rm IR} + 12M_5^3 - \frac{1}{8}\alpha^2)/(12M_5^3)$ and $\tau_{\rm IR}$ is the tension of the IR boundary which can be de-tuned away from the RS value of $-12M_5^3$. The above potential has a minimum at $\langle\phi\rangle$ which is hierarchically smaller than $\Lambda_{\rm UV}$ [31, 33],

$$\frac{\langle\phi\rangle}{\Lambda_{\rm UV}} \equiv \frac{\Lambda_{\rm IR}}{\Lambda_{\rm UV}} = \left(\frac{12M_5^3\lambda}{\alpha v}\right)^{\frac{1}{\epsilon}}. \tag{3.10}$$

[3] Note, to get the UV boundary condition we assumed $\kappa \gg 1$.

Here, V_1 is a constant energy density that will be determined below. The parameter ϵ controlling the hierarchy is determined by the mass of the Goldberger-Wise field,

$$\epsilon = -2 + \sqrt{4 + m^2} \underset{m^2 \ll 1}{\approx} m^2/4. \tag{3.11}$$

Requiring small back reaction of the Goldberger-Wise field to the AdS-S geometry requires $\lambda, \epsilon < 1$. If we think of $\Lambda_{\rm UV}$ being of the order of highest scales $\sim M_{\rm Pl}$, and $\Lambda_{\rm IR} \gtrsim$ TeV, so as to solve the Hierarchy Problem, this large hierarchy can emerge from modest parameters with $12M_5^3\lambda/(\alpha v)$ and ϵ being $O(0.1)$. To get the free energy, we note that for $T \ll \phi$, the KK modes are not excited and $\phi(x)$ is the only dynamical light field in the confined phase. Thus the above effective potential also gives the free energy of the confined phase,

$$F_{\rm confined} \underset{T \ll \phi}{\approx} V_{\rm rad}(\phi). \tag{3.12}$$

Let us now relate the two constant energy densities appearing in eqs. (3.5) and (3.12). We require that the two geometries given by eqs. (3.2) and (3.3) match when $\rho_h \to 0$ and $\phi \to 0$ since in that case they both describe zero temperature with the IR boundary removed (to $\rho = 0$). Thus the two free energies given in eqs. (3.12) and (3.5) should also match when $T \to 0$ and $\phi \to 0$, thereby making $V_0 = V_1$. We can now calculate the temperature at which the two free energies in eqs. (3.5)

and (3.12) become equal, namely the critical temperature for the PT, T_c:

$$F_{\text{deconfined}}(T_c) = F_{\text{confined}}(T_c) \;\Rightarrow\; \frac{T_c}{\Lambda_{\text{IR}}} = \left(\frac{-6\epsilon\lambda}{\pi^4(4+\epsilon)}\right)^{1/4}. \tag{3.13}$$

Thus T_c is parametrically smaller than Λ_{IR} for small ϵ and(or) small λ. This justifies the effective description of the confined phase involving only the radion as well as eq. (3.8). Furthermore, the above fact indicates that at the temperature T_c we can have a simultaneous existence of both the confined and the deconfined phases, and thus the PT under consideration is first order in nature. It follows from eq. (3.13) that $V_0 = 2\pi^4 M_5^3 T_c^4$ for the almost vanishing cosmological constant today i.e. at $\phi = \langle\phi\rangle$.

The semi-classical bounce solution that we will compute in the next section will correspond to quantum tunneling in terms of the gravitational radius ρ_h, but in terms of T (to match with CFT expectations), it will correspond to a thermal transition as is clear from the presence of $\hbar$ in eq. (3.4).

3.2 The structure of the bounce

As discussed in the previous section, the effect of 4D gravity can be approximated by an adiabatic adjustment of the temperature T and the Hubble parameter H. Starting at high T and in the AdS-S phase as the universe expands, T eventually drops below T_c. As this happens, the RS phase having a smaller free energy, becomes thermodynamically favorable and bubbles of the RS phase can start nucleating. The phase transition completes only after the bubbles start percolating, and

this happens when the rate of bubble nucleation per unit volume, Γ, gets bigger than H^4. For $T \ll T_c$, H asymptotes to a constant given by $H^2 \approx \frac{8\pi}{3} G_N V_0 \sim \frac{2\pi^4 M_5^3 T_c^4}{3M_{\rm Pl}^2}$. Here, G_N and $M_{\rm Pl}$ are respectively Newton's constant and the reduced Planck scale, $M_{\rm Pl} = 2.4 \times 10^{18}$ GeV. To find the temperature at which the phase transition completes, we need to compute the nucleation rate Γ. Since the 5D theory is weakly coupled, we can use a semiclassical approximation to compute Γ in terms of a Euclidean bounce action $S_{\rm b}$ as,

$$\Gamma \sim T^4 e^{-S_{\rm b}}. \tag{3.14}$$

Thus for the PT to complete one needs roughly

$$S_{\rm b} < 4 \ln \left(\frac{M_{\rm Pl}}{T_c} \right) \sim 140, \tag{3.15}$$

where we used $T_c \sim \mathcal{O}(\text{TeV})$.

To compute the bounce action, in principle, one has to look for a solution of the Euclidean equation of motion (EoM) derived from the 5D action (3.1) that smoothly interpolates between the two above mentioned geometries in eqs. (3.3) and (3.2) (with time compactified on a circle of circumference $1/T$). Authors of ref. [3] attempted to make this trade at the common RS2 limit of both phases (RS2 is the $\Lambda_{\rm IR} = 0$ limit of RS1 and also the limit $T = 0$ of AdS-S). They then tried to derive the RS1 phase of the bubble interior by solving the Euclidean EoM within the 4D radion EFT (up to two derivative order). Qualitatively, their results are shown in

figure 3.2. In most of the interior region, the 4D radion EFT bounce is controlled and approximates the true 5D bounce. However, as pointed out in ref. [3], the central problem with this proposed bounce solution is that it goes out of 4D radion EFT control as one approaches the RS2 juncture (shown in gray in figure 3.2) since the IR scale ϕ becomes smaller than T. Indeed, the lack of smoothness of the brane at the RS2 point takes this bounce configuration outside even 5D EFT control. The interpolation from RS2 to AdS-S is similarly out of the 5D EFT control.

By contrast, we will consider a *smooth* bounce configuration as illustrated in figure 3.2. As in figure 3.2, the interior region is described by a bounce solution in 4D radion EFT, but deviates from figure 3.2 for $\phi \sim T$ near the transition regime (shown in gray in figure 3.2), with the brane capped off smoothly so that it is controlled within 5D EFT. With this smoothness criterion, which we will elaborate further below, finding the bounce solution is a mathematically well-posed question. However the exact solution is difficult to find in practice.[4] Instead, we will proceed by making a reasonable *ansatz* for the 5D geometry of the bounce that satisfies the same smoothness criterion. Although such an ansatz may not be the true bounce solution, (a) we will argue later that in the thin-wall regime,

$$S_{\text{b, ansatz}}^{\text{thin-wall}} > S_{\text{b, true}}^{\text{thin-wall}}, \tag{3.16}$$

so it can provide an upper bound for $S_{\text{b, true}}^{\text{thin-wall}}$ and hence a lower bound for Γ; (b) it

[4]Nevertheless, see our remarks in the introduction regarding the possibility of obtaining the actual bounce solution in the thin-wall limit for a 6D example [60], taking advantage of a symmetry between the Euclidean time circle and the sixth dimension.

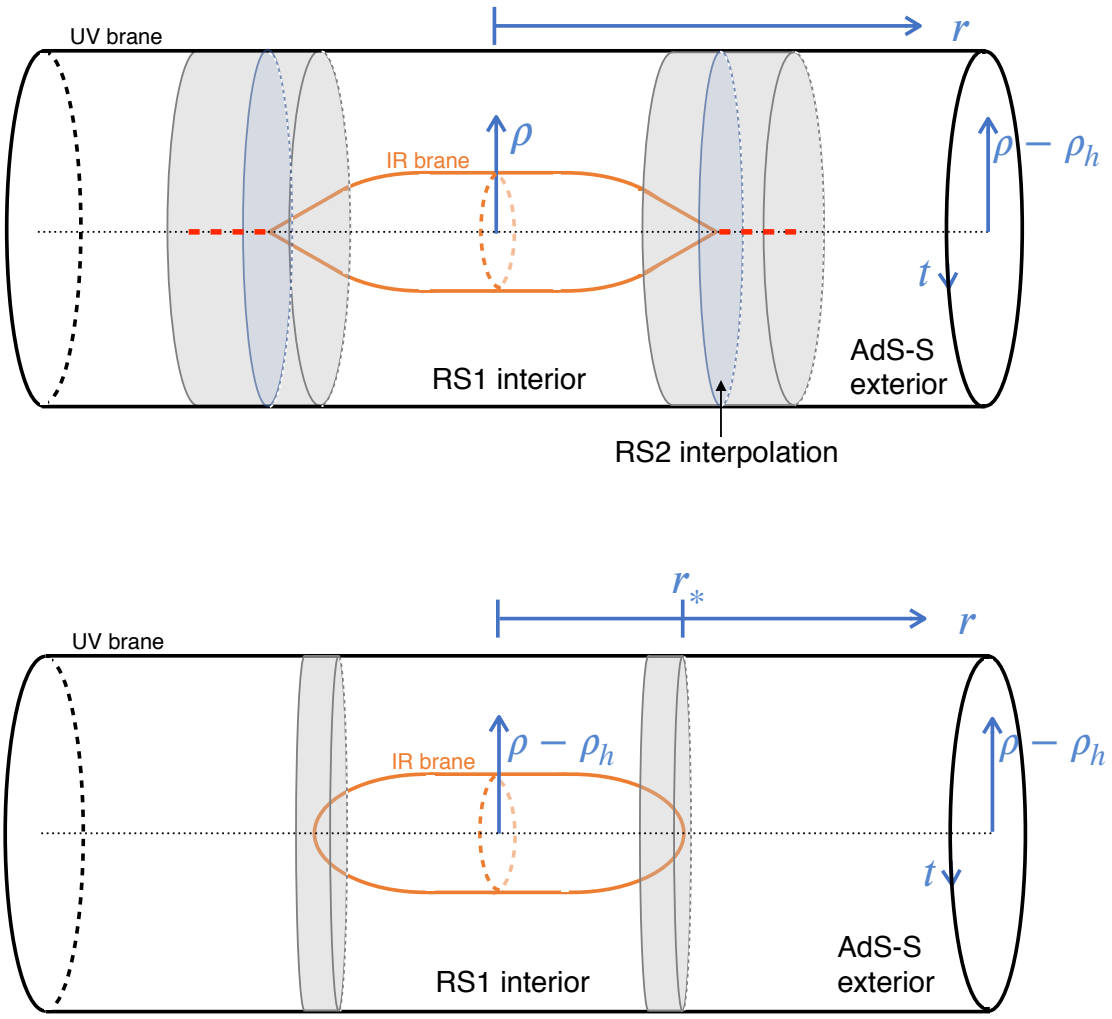

Figure 3.1: (a) Topology of the bounce proposed in ref. [3]. In the gray region the description of the ansatz gets out of 4D radion EFT as well as 5D EFT control. The orange surface shows the IR brane, and the red dashed line indicates the adjustment of ρ_h between its equilibrium AdS-S value to zero at the RS2 limit. (b) Smooth bounce topology/configuration proposed in this work, describable within 5D EFT. The IR brane (the orange surface) is smoothly capped off at the horizon. In the gray region, the (two-derivative) 4D radion EFT gets out of control, but the bounce can still be described within 5D EFT.

provides a reasonable estimate for Γ more generally.

For the smooth ansatz we consider in this paper, the entire configuration can be described as globally AdS-S with the region inside the IR brane "cut-out". In

particular, the RS1 phase in the far interior is being approximated by the IR brane cutting out a portion of AdS-S rather than a zero temperature AdS. This is a good approximation because in the far interior $\phi \gg T$. The key to smoothness of our ansatz, and hence 5D EFT control, is that the brane is capped off at the horizon $\rho = \rho_h$ as opposed to at $\rho = 0$ as in ref. [3]. However, we make no claim that the smooth transition region, shown in gray, is a controlled approximation to the true bounce in that it does not solve the 5D Euclidean EoM. Rather, it is a qualitatively accurate ansatz, which smoothly interpolates controlled approximations in the far interior and the far exterior indicated in white region in figure 3.2. As pointed out above, in the thin-wall limit this ansatz will provide us a lower bound on the true nucleation rate while outside this limit, the ansatz can be expected to give us a reasonable estimate of this rate.

In more detail, we take our ansatz for the bounce to be described by

$$ds^2 = \left(\rho^2 - \frac{\rho_h^4}{\rho^2}\right) dt^2 + \frac{d\rho^2}{\rho^2 - \frac{\rho_h^4}{\rho^2}} + \rho^2 \sum_i dx_i^2, \tag{3.17}$$

with $\rho_h < \phi(r) < \rho < \Lambda_{\rm UV}$ for $r \equiv |\vec{x}| < r_*$ and $\rho_h < \rho < \Lambda_{\rm UV}$ for $r > r_*$. Here $\phi(r)$ changes between some release point $\phi_r \gg \rho_h$ at $r = 0$ and ρ_h at r_*, describing an r-dependent IR brane end to the extra dimension in the region $r < r_*$.[5] We see that in the far exterior this is the AdS-S metric and in the far interior, since $\phi_r \gg \rho_h$, this approximates RS1 at very low temperatures eq. (3.2). This gives an $O(3)$ symmetric ansatz for the bounce, schematically shown in figure 3.2. The justification for a time

[5] In the thin-wall regime, $\phi_r = \langle\phi\rangle$, but away from the thin-wall regime, ϕ generally approaches a $\phi_r < \langle\phi\rangle$ at $r = 0$

independent $O(3)$ symmetric bounce structure arises as a result of (two derivative) radion dominance of the bounce action and is given in ref. [1]. Note that the choice $\phi(r_*) = \rho_h$ implies that the IR brane is pinching off to zero time circumference at r_* so that we have a closed IR brane hypersurface. It remains to choose a specific $\phi(r)$ that this pinching off results in a *smooth* brane embedding seen in figure 3.2.

We will first show how to compute the action eq. (3.1) for a given $\phi(r)$. We will then discuss the conditions that ensure a smooth ansatz and minimize the action subject to those conditions to obtain the ansatz (i.e. $\phi(r)$) that gives us the strongest upper bound on the bounce action in the thin-wall limit. We now proceed by computing different terms in the action eq. (3.1). To obtain the extrinsic curvature K, we first find the unit normal vector to the surface $\rho = \phi(r)$,

$$n_\phi = \left(\frac{\rho^2}{\rho^4 - \rho_h^4 + \phi'^2}\right)^{1/2} (0, -\phi', 0, 0, 1), \tag{3.18}$$

where $\phi' \equiv \frac{d\phi}{dr}$. The induced metric on this surface is given by

$$ds^2_{\text{ind}} = \left(\rho^2 - \frac{\rho_h^4}{\rho^2}\right) dt^2 + \left(\rho^2 + \frac{\phi'^2}{\rho^2 - \frac{\rho_h^4}{\rho^2}}\right) dr^2 + \rho^2(r^2 d\theta^2 + r^2 \sin^2\theta d\varphi^2). \tag{3.19}$$

From the above the trace of the extrinsic curvature and the determinant of the

induced metric can be calculated as,

$$\sqrt{\gamma} = r^2 \sin\theta \phi^2 \left(\phi^4 - \rho_h^4 + \phi'^2\right)^{1/2}, \tag{3.20}$$

$$\sqrt{\gamma}K = r^2 \sin\theta \frac{1}{\phi^4 - \rho_h^4 + \phi'^2} \times \left[2\phi(\rho_h^4 - \phi^4)\frac{\phi'}{r} + (6\phi^4 - 2\rho_h^4)\phi'^2 - 2\phi\frac{\phi'^3}{r} + (\phi^4 - \rho_h^4)(4\phi^4 - 2\rho_h^4 - \phi\phi''(r))\right]. \tag{3.21}$$

Using the above we can evaluate the full action in eq. (3.1) as a function of $\phi(r)$ to get,

$$S_\phi = \frac{4\pi}{T}\int dr r^2 \left[2M_5^3\Big(\frac{2}{\phi^4 - \rho_h^4 + \phi'^2}\left[2\phi(\rho_h^4 - \phi^4)\frac{\phi'}{r} + (6\phi^4 - 2\rho_h^4)\phi'^2 - 2\phi\frac{\phi'^3}{r} + (\phi^4 - \rho_h^4)(4\phi^4 - 2\rho_h^4 - \phi\phi'')\right] + \rho_h^4 - 2\phi^4 - 6\phi^2\left(\phi^4 - \rho_h^4 + \phi'^2\right)^{1/2}\Big) + V_{\rm rad}(\phi)\right], \tag{3.22}$$

where $V_{\rm rad}(\phi)$ is the contribution coming from S_χ. For $\rho > \phi \gg \rho_h$ (the white interior region in figure 3.2 outside the orange surface), the AdS-S geometry, the low temperature RS geometry, and the zero temperature RS geometry are all approximately the same and $V_{\rm rad}(\phi)$ becomes the standard zero temperature radion potential given in eq. (3.9). In this regime and for $\phi' \ll \phi^2$, the effective action (3.22) reduces to the standard two derivative radion action in the Euclidean time independent $O(3)$ symmetric regime,

$$S_\phi \approx \frac{4\pi}{T}\int dr r^2 \Big[6M_5^3\phi'^2 + V_{\rm rad}(\phi)\Big]. \tag{3.23}$$

In this $\phi \gg \rho_h$ region, the solution to the EoM derived from the above action is a controlled approximation to the true bounce and gives the parameterically dominant contribution to the bounce action, as anticipated in refs. [1, 3] and fully justified in section 3.3. However, the solution itself takes us out of radion EFT into the region $\phi \sim \rho_h$ (shown in gray in figure 3.2). For $\phi \sim \rho_h$, although it is not straightforward to calculate the contribution of S_χ in detail, its contribution to S_ϕ is suppressed by the parameter λ (see eq. (3.9)), whereas the rest of the terms in S_ϕ are *un*suppressed, as can be seen using eq. (3.22). Thus for $\phi \sim \rho_h$, $V_{\rm rad}(\phi)$ will not play a significant role in determining the bounce and we will keep using the same $V_{\rm rad}(\phi)$ given in eq. (3.9) even in this region for convenience. The contribution of S_χ to terms involving ϕ' is also suppressed by λ compared to terms arising from 5D gravitational action $S_{\rm GR}$ and thus has been neglected in eq. (3.22).

To find the optimal form of $\phi(r)$ for our anstaz (eq. 3.17 and discussion below it, figure 3.2) in the thin-wall limit we will choose $\phi(r)$ to minimize the bounce ansatz action eq. (3.22) by solving the "EoM" that follows from it. We show an example of such a solution in figure 3.2. For this solution, the 5D geometry is smooth everywhere except in the potentially problematic region where the IR boundary merges into the AdS-S horizon ($r \approx r_*$ region in figures 3.2 and 3.2). To see whether this merging is smooth, we evaluate the induced metric in the near-horizon region by writing $\phi(r) = \rho_h + \delta\phi(r)$. Assuming $\rho_h^3 \delta\phi \ll \phi'^2$, we get

$$ds^2_{\rm ind} \supset 4\rho_h \delta\phi dt^2 + \frac{\phi'^2}{4\rho_h \delta\phi} dr^2 = 4\rho_h^2 y^2 dt^2 + dy^2, \tag{3.24}$$

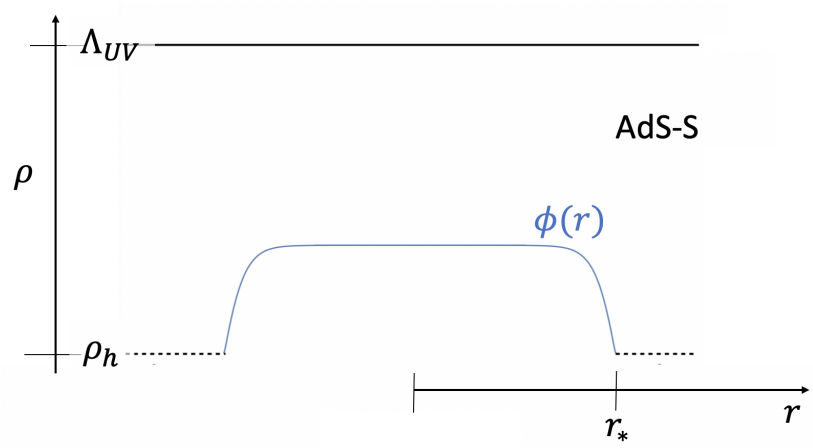

Figure 3.2: An example of the profile of the bounce ansatz, obtained by solving the EoM resuling from the action of eq. (3.22). The black dashed lines represents the black-brane horizon and the blue curve shows the IR-brane profile specified by $\phi(r)$.

where we have made the change of variable/coordinate $y = \sqrt{\delta\phi/\rho_h}$. Note that this is the same as the metric of a flat space with the correct time periodicity. This piece of flat space is embedded in AdS-Schwarzchild, with (near horizon) metric

$$ds^2 = 4\rho_h^2 y^2 dt^2 + dy^2 + \rho_h^2 \left(dr^2 + r^2 \left(d\theta^2 + \sin^2\theta d\varphi^2\right)\right), \tag{3.25}$$

at a fixed r. This ensures a smooth brane, smoothly embedded in AdS-S, with two coordinates/directions t and r acting as spectators, analogous to embedding of a 2D sphere in 3D flat space.

For concreteness, we will choose the boundary condition

$$\phi'|_{\phi=\rho_h} = \rho_h^2 \tag{3.26}$$

for our ansatz which respects the above condition $\rho_h^3\delta\phi \ll \phi'^2$ near the horizon, en-

suring a smooth brane embedding. This condition, along with the usual smoothness condition at the bubble center, $\phi'|_{r=0} = 0$, fixes our ansatz.[6]

3.3 Phase transition in thin-wall regime

Having discussed the effective action (3.22) for ϕ and the boundary conditions needed to fix the solution, we can now calculate the bounce action based on our ansatz. Although one can proceed numerically in general, in the thin-wall regime ($T \approx T_c$) it is possible to obtain an analytical expression for the bounce action.

As mentioned before, we focus on the bounce action with $O(3)$ symmetry. The $O(3)$ symmetric bounce action can be rewritten quite generally in the thin-wall regime as [55, 56],

$$S_{\rm b} = \frac{S_3}{T} = \frac{16\pi}{3}\frac{S_1^3}{(\Delta F)^2 T}, \tag{3.27}$$

where ΔF is the difference of the free energy in two phases. S_1 is the surface tension of the bubble wall, evaluated in the degenerate limit $\Delta F = 0$. Therefore, any configuration of S_1 is always bounded from below. Finding the true solution of S_1 is basically minimizing S_1. Any other ansatz, which is not the solution, should satisfy $S_{1,\rm ansatz} > S_{1,\rm true}$. Combining with eq. (3.27), this leads to $S_{\rm b,ansatz} > S_{\rm b,true}$. However, a random $S_{\rm b,ansatz}$ might involve singularities which take us outside 5D EFT control. In this regard, our smooth ansatz (figure 3.2) provides a controlled upper bound on the true bounce action in the thin-wall limit.

[6] We note that although the action eq. (3.22) involves ϕ'', the EoM obtained from it is still a second order differential equation for $\phi(r)$ and so (only) two boundary conditions are needed to fix its solution.

For our ansatz, the surface tension of the bubble S_1 can be obtained from eq. (3.22) as,

$$S_1 = \int dr \left[2M_5^3 \left(\frac{2\left[(6\phi^4 - 2\rho_h^4)\phi'^2 + (\phi^4 - \rho_h^4)(4\phi^4 - 2\rho_h^4 - \phi\phi'')\right]}{\phi^4 - \rho_h^4 + \phi'^2} \right.\right.$$
$$\left.\left. + \rho_h^4 - 2\phi^4 - 6\phi^2 \left(\phi^4 - \rho_h^4 + \phi'^2\right)^{1/2} \right) + V_{\rm rad}(\phi) \right]. \tag{3.28}$$

To clearly show the parametric dependence of S_1, we divide it into two parts: $S_1 = S_1^{\rm radion} + S_1^{\rm transition}$, where $S_1^{\rm radion}$ is the part of bounce action deep inside the bubble (see the white interior of figure 3.2), where 4D radion EFT (eq. (3.23)) is valid, while $S_1^{\rm transition}$ denotes the contribution in the transition region $\phi \sim \rho_h$, where the 5D EFT is needed (the gray region of figure 3.2). As shown around eq. (3.23), in the interior of the bubble, where $\phi \gg \rho_h$ and $\phi^2 \gg \phi'$, $S_1^{\rm radion}$ reduces to the one dimensional radion action

$$S_1^{\rm radion} \approx \int_0^{\lesssim r_*} dr \left[6M_5^3\phi'^2 + V_{\rm rad}(\phi)\right] \approx \sqrt{24M_5^3} \int_{\gtrsim \rho_h}^{\langle\phi\rangle} d\phi \sqrt{V_{\rm rad}(\phi)}$$
$$\approx 0.9\,(16\pi^2 M_5^3) \left(\frac{1}{\epsilon\lambda}\right)^{1/4} T_c^3 \quad (\epsilon\lambda \ll 1) \tag{3.29}$$

where the equality in the first line follows from the EoM. One of the integration limits is fixed because the bounce action starts at the minimum of the potential ($\phi = \langle\phi\rangle$). As ϕ approaches ρ_h, the approximation in eq. (3.29) breaks down and therefore we stop the integration at $\phi \gtrsim \rho_h$. In the second line of eq. (3.29), we used eq. (3.13) to rewrite $\langle\phi\rangle$ in terms of T_c. It is clear from eq. (3.29) that $S_1^{\rm radion}$ is enhanced for small ϵ and/or λ.

The expression for $S_1^{\text{transition}}$ is hard to obtain analytically but one can easily get its parametric dependence. Given $\phi \sim \rho_h$ and $\phi' \sim \rho_h^2$ in the transition region, all terms in $S_1^{\text{transition}}$ are of order $M_5^3 \rho_h^3$ (see eq. (3.28)). Therefore, $S_1^{\text{transition}} \sim M_5^3 T_c^3$ and it is parametrically smaller than S_1^{radion} for small ϵ and/or λ. Now we can conclude that, for small ϵ and/or λ, $S_1 \approx S_1^{\text{radion}}$, which means the bounce action is dominated by the contribution from standard radion EFT (up to two derivative order). Plugging S_1^{radion} in to eq. (3.27), S_{b} is therefore given as

$$S_{\text{b}} \approx 8\,(16\pi^2 M_5^3)\left(\frac{1}{\epsilon\lambda}\right)^{3/4} \frac{T_c/T}{\left((1-(T/T_c)^4\right)^2} \qquad (\epsilon\lambda \ll 1). \tag{3.30}$$

The radion EFT dominance is also justified based on some benchmark points in table 3.1.

Model parameters	$S_1/(16\pi^2 M_5^3 T_c^3)$	$S_1^{\text{radion}}/(16\pi^2 M_5^3 T_c^3)$	$S_{\text{b}}/(16\pi^2 M_5^3)$
$\epsilon = 1/2, \lambda = 1/2$	1.2	0.5	90
$\epsilon = 1/25, \lambda = 1/2$	2.1	1.3	486
$\epsilon = 1/25, \lambda = 1/25$	4.1	3.3	3.7×10^3
$\epsilon = 1/100, \lambda = 1/100$	8.7	7.8	3.4×10^4

Table 3.1: Comparison of numerical results of S_1 (eq. (3.28)) and S_1^{radion} (eq. (3.29)) for different model parameters ϵ , λ. To get the concrete number for S_1^{radion}, we set the lower integration limit to ρ_h in the first line of eq. (3.29). We also show the full bounce action S_{b} (eq. (3.27)) in the thin-wall limit in terms of S_1 at $(T/T_c)^4 = 1/2$.

We see that, while for very small ϵ and λ, radion dominance gives a quantitatively good approximation, for small but not very small ϵ and λ, the approximation is poor. In these cases of interest, our ansatz in the full 5D theory is key to providing a rigorous bound on the true bounce action.

In the above, we have described the general considerations of PT dynamics

in the thin-wall limit. However, when we apply them to the real world, we find that the thin-wall limit is incompatible with the observed Planck-Weak hierarchy. Concretely, with $\lambda \lesssim 1$ to ensure a controlled back-reaction, and $\epsilon = 1/25$ to obtain the large Planck-Weak hierarchy, we see that the PT does not complete near T_c even for $16\pi^2 M_5^3 = 1$ as can be seen using eq. (3.15). However, for theoretical control of the 5D EFT we need $16\pi^2 M_5^3 > 1$.[7]

However, non-minimal models can improve the compatibility with the thin-wall limit. To allow the PT to happen for larger values of M_5^3, we need larger values of ϵ (see the first line of table 3.1) while still generating the correct value of the Planck-Weak hierarchy. We will introduce a scenario which achieves these goals in the next section.

3.4 5D realization of the two-FP model

In the previous chapter, we proposed a scenario from the dual (near-)CFT perspective with distinct UV and IR fixed points, which can simultaneously achieve a large Planck-Weak hierarchy and also have a larger ϵ controlling the PT, such that it can complete promptly in a theoretically controlled parameter regime.

In this section, we will realize the above scenario in a simple explicit 5D model utilizing an *interacting* Goldberger-Wise stabilizing field, and show that it indeed leads to a relatively prompt PT consistent with a large Planck-Weak hierarchy. This will enable us to obtain explicit expressions of various 4D parameters such as ϵ, ϵ'

[7] This is just a requirement that the quantum gravity loops or $\sim 1/(16\pi^2 M_5^3)$ corrections are small at the AdS curvature scale.

etc. described above, in terms of fundamental 5D parameters, utilizing which we will calculate the rate of the PT.

We consider the following Goldberger-Wise potential,

$$V_\chi = \frac{1}{2}m'^2\chi^2 + \frac{1}{6}\eta\,\chi^3 + \frac{1}{24}g\,\chi^4, \tag{3.31}$$

where m' is the mass of the Goldberger-Wise scalar and η, g are two coupling constants. The EoM for the extra-dimensional profile of the Goldberger-Wise field in the RS metric of eq. (3.2) is given by

$$\rho^5\partial_\rho^2\chi + 5\rho^4\partial_\rho\chi - \rho^3 V'_\chi = 0. \tag{3.32}$$

For later purposes it is convenient to do a coordinate transformation, $\rho = \Lambda_{\rm UV}e^{-\sigma}$ with $0 < \sigma < L \equiv \ln(\Lambda_{\rm UV}/\Lambda_{\rm IR})$, following which the EoM reads as,

$$\partial_\sigma^2\chi - 4\partial_\sigma\chi - V'_\chi = 0. \tag{3.33}$$

The above EoM indicates that there exist FP solutions in the extra-dimensional evolution of the Goldberger-Wise profile. They appear where $\chi =$ constant : $V'_\chi(\chi) = 0$ and are located at non-negative values

$$\chi = 0 \text{ and } \chi = \chi_* = \frac{3}{g}\left(-\frac{\eta}{2} + \sqrt{\frac{\eta^2}{4} - \frac{2gm'^2}{3}}\right), \tag{3.34}$$

for $m'^2, \eta < 0$ and $g > 0$.

Obtaining the analytical expression for the full radion action from the general Goldberger-Wise potential in eq. (3.31) is challenging. However, we can obtain the relevant qualitative insights about the behavior of the Goldberger-Wise profile under eq. (3.31) by using the two-FP intuition described in the previous subsection.

In the proximity of the FPs at $\chi = 0$ and $\chi = \chi_*$, the field profile evolves quite slowly, whereas as it evolves rapidly near the transition from the vicinity of one FP to the other. Hence, as a simple approximation, we can split the evolution of χ into two regimes. In the first regime i.e. for field values between $0 \leq \chi < \chi_{\rm m}$, we consider the evolution to be governed by the FP at $\chi = 0$, and hence with a potential $\frac{1}{2}m'^2\chi^2$. For the other segment i.e. for field values between $\chi_{\rm m} < \chi \leq \chi_*$, the evolution is governed by the FP at $\chi = \chi_*$ and hence with a potential $\frac{1}{2}m^2(\chi - \chi_*)^2$ where $m^2 \equiv V''_\chi(\chi_*) = -2m'^2 - \eta\chi_*/2$. We choose to match two regimes at a field value $\chi_{\rm m} = (-\eta + \sqrt{\eta^2 - 2gm'^2})/g$, which is the inflection point of $V(\chi)$. To summarize, we consider the simplified Goldberger-Wise potential $\tilde{V}_\chi$,

$$\tilde{V}_\chi(\chi) \approx \begin{cases} \frac{1}{2}m'^2\chi^2 & \text{for } 0 \leq \chi < \chi_{\rm m} \\ \\ \frac{1}{2}m^2(\chi - \chi_*)^2 - C & \text{for } \chi_{\rm m} < \chi \leq \chi_*. \end{cases} \tag{3.35}$$

In the above, $C = \frac{1}{2}m^2(\chi_{\rm m} - \chi_*)^2 - \frac{1}{2}m'^2\chi_{\rm m}^2$ is a constant that ensures the continuity of $\tilde{V}_\chi$ at $\chi_{\rm m}$.

A comparison of the numerical solution obtained for the full potential in eq. (3.31) with the simplified potential in eq. (3.35) is shown in figure 3.3. Here we choose the same boundary conditions as in eq. (3.7) with $0 < v < \chi_{\rm m}$, $\alpha > v$

and fix $L = 15\pi$. Figure 3.3 clearly shows the asymptotic behaviour of $\chi(\sigma)$ near $\chi = 0$ and χ_*, which act as the UV and IR fixed points with respect to the flow in the extra dimension that is dual to the RG flow in the CFT perspective. As can be seen from figure 3.3, the simplified potential gives a good approximation to the full potential, and correspondingly we can trust the analytical calculation of the radion potential using eq. (3.35).

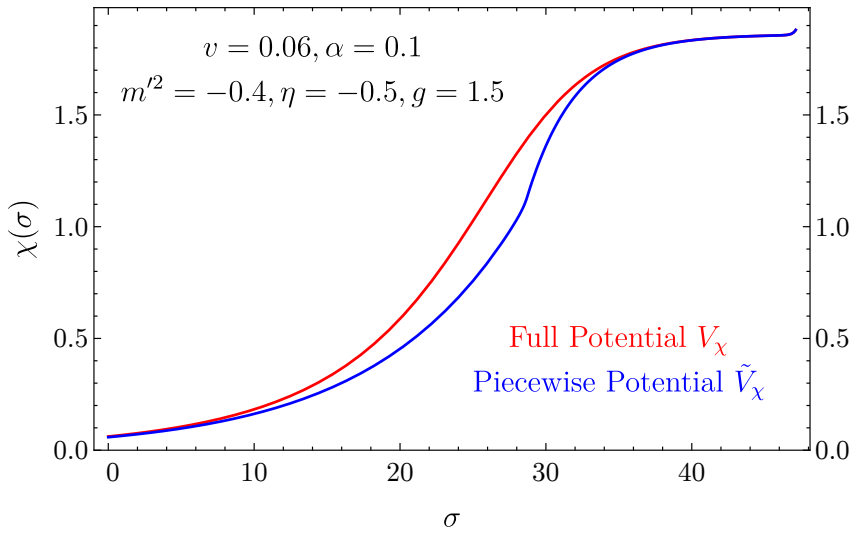

Figure 3.3: The profile of Goldberger-Wise scalar $\chi(\sigma)$ from two different potentials: full potential eq. (3.31) and simplified potential eq. (3.35) . The parameters we choose are $m'^2 = -0.4$, $\eta = -0.5$, $g = 1.5$ and v=0.06, $\alpha = 0.1$ and $L = 15\pi$.

Given the quadratic piecewise Goldberger-Wise scalar potential in eq. (3.35), the radion potential can be calculated analytically (see details in appendix C), which can be summarized as

$$V_{\text{rad}}(\phi) \approx \begin{cases} \tau\phi^4 - \alpha v \phi^{4-\epsilon'} & \phi > \phi_{\text{m}} \\ (\tau - \alpha\chi_*)\phi^4 + \frac{\alpha\chi_{\text{m}}}{2}\left(\frac{\chi_{\text{m}}(1-\frac{\epsilon}{8})}{v}\right)^{\epsilon/\epsilon'} \phi^{4+\epsilon} & \phi \ll \phi_{\text{m}} \end{cases}, \tag{3.36}$$

In eq. (3.36), $\tau = \delta\tau_{\rm IR} - \frac{1}{8}\alpha^2$ is determined in terms of detuning on the IR boundary $\delta\tau_{\rm IR} \equiv \tau_{\rm IR} + 12M_5^3$, $\epsilon' = 2 - \sqrt{4+m'^2}$ and ϵ is defined in eq. (3.11). Finally, $\phi_{\rm m} \equiv e^{-L_{\rm m}}$ where $L_{\rm m}$ is the smallest size of the extra dimension where the Goldberger-Wise profile reaches the value $\chi_{\rm m}$ on the IR boundary. For $L < L_{\rm m}$, $\chi(\sigma)$ never grows to reach $\chi_{\rm m}$ in the extra dimension, whereas for $L > L_{\rm m}$, $\chi(\sigma)$ becomes bigger than $\chi_{\rm m}$ and goes to the vicinity of the IR FP near the IR boundary.

We can choose the parameters such that the radion potential above has only one minimum for $\phi < \phi_{\rm m}$ at

$$\langle\phi\rangle \sim \left(\frac{v}{\chi_{\rm m}(1-\epsilon/8)}\right)^{1/\epsilon'} \left(\frac{-2\tau'}{\alpha\chi_{\rm m}}\right)^{1/\epsilon}, \tag{3.37}$$

where $\tau' \equiv \tau - \alpha\chi_* < 0$. This expression of the hierarchy is to be compared with eq. (3.10) in the single-FP scenario. The large Planck-Weak hierarchy can be obtained from the first factor of the RHS of eq. (3.37) with a small $\epsilon' \sim 1/25$ and a modest ratio of v/χ_*,[8] while now allowing ϵ to be considerably larger. As shown in section 3.2, it is the region $\phi \lesssim \langle\phi\rangle < \phi_{\rm m}$ that is relevant for PT dynamics and is controlled by ϵ. Consequently, our computation of the bounce action obtained in the previous sections using eq. (3.9) can be applied, but now with only modestly small $\epsilon \lesssim 1$, thereby achieving the goal stated at the end of section 3.3. Correspondingly for $\epsilon > \epsilon'$, the bounce action in the thin-wall regime becomes parametrically smaller, as suggested by eq. (3.30), and this allows for the PT to complete for parametrically larger N.

[8] As we explain in appendix C, the radion potential in eq. (3.36) has been obtained with the approximation that the second factor of the RHS of eq. (3.37) is $\lesssim 0.1$.

As discussed earlier, the bounce in the thin-wall regime encompasses $\phi \leq \langle\phi\rangle < \phi_{\rm m}$. Thus we can directly use the second line of eq. (3.36) to calculate the bounce. Given the exact similarity between this potential and the one in eq. (3.9), used to calculate bounce action in section 3.3, we can directly re-use the results given in table 3.1, even though such results were obtained in a single-FP scenario.

Having worked out these general features of the thin-wall regime in our two-FP scenario, with the rigorous bounds following from our ansatz, we now apply them to the case of a realistic PT consistent with the Planck-Weak hierarchy. For a benchmark set of parameters $\epsilon = 0.5, \lambda = 0.5$, as shown in table 3.1, the PT can complete promptly for $16\pi^2 M_5^3 \gtrsim 1$ in the thin-wall regime, (marginally) under theoretical control. This was completely impossible in the original single-FP scenario mentioned in section 3.3.

For the regions of parameter space that the PT does not complete near T_c, the universe keeps cooling down to temperatures where the thin-wall approximation is no longer valid. In the next section we will consider such transition temperatures outside the thin-wall regime, with even better semi-classical control.

3.5 Phase transition outside thin-wall regime

We now study the bounce for smaller T, where the thin-wall approximation is not valid and our ansatz bounce can no longer be shown to be a rigorous upper bound on the true bounce action. However, our bounce ansatz smoothly and simply interpolates the two phases and should still provide a very reasonable estimate

of the true bounce action. Therefore, we will continue to use eq. (3.22) and the boundary conditions mentioned in and around eq. (3.26) to numerically obtain the $O(3)$ symmetric bounce action S_3 for all temperature (see solid lines in figure 3.4). In figure 3.4 we also show the bounce action found using the two-derivative 4D EFT of the dilaton (dual to radion of the 5D theory). As we discussed in [1], the bounce action is dominated by such an EFT for small ϵ and λ. This is dual to the radion two-derivative EFT dominance in our 5D ansatz for small ϵ and λ, as discussed before. To compare the two-derivative approximation to our full 5D results in this paper, we use the radion EFT Lagrangian shown in eq. (3.23) and follow the same strategy as in [1] to determine one of the boundary conditions as $\phi'|_{\phi=0} = \sqrt{\pi^4 T^4/3}$ and thereby solve the bounce. Note that this choice extends into the region $\phi < T$ where the two-derivative EFT clearly breaks down. However, since $T < T_c \ll \langle\phi\rangle$ for small ϵ and λ, the contribution from this uncontrolled region is parametrically small and can be viewed as a subleading correction to the true bounce. As shown in figure 3.4, the bounce action S_3 calculated by the 4D two-derivative EFT and the full 5D ansatz agree for small ϵ and λ, as expected from the argument in [1]. On the other hand, for larger λ ($\lambda = 0.5$) we see from figure 3.4 that the two-derivative approximation is only very crude and the full 5D treatment is required.

Having considered the general structure and parametrics of the PT dynamics, we now consider values of ϵ and λ such that the observed Planck-Weak hierarchy and a successful PT are achieved. This will necessitate values of ϵ and λ large enough that the two-derivative radion dominance approximation is insufficient and a fully 5D treatment is necessary. The 5D bounce is at least mathematically soluble in

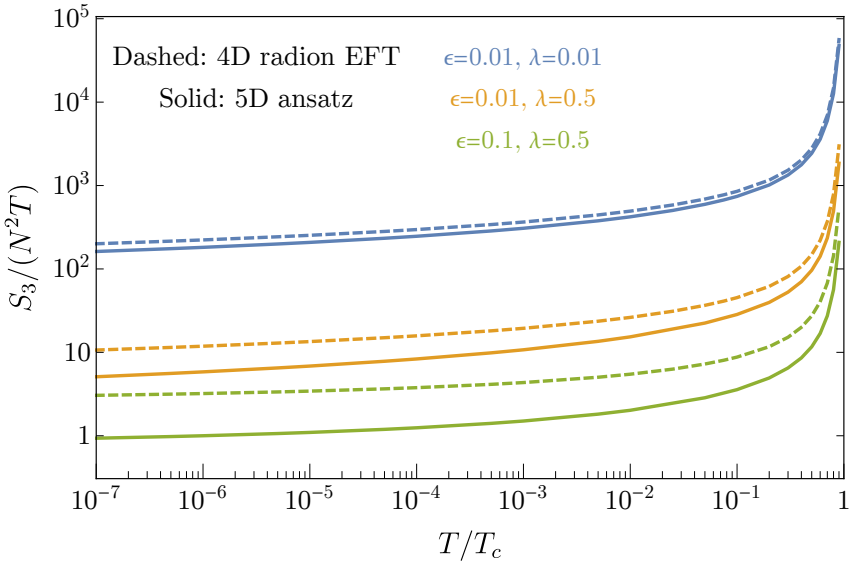

Figure 3.4: The $O(3)$ symmetric bounce action $S_3/(N^2T)$, where $N \equiv \sqrt{16\pi^2 M_5^3}$, as a function of temperature T/T_c for different choices of ϵ and λ. The solid lines denote the results using 5D ansatz, while the dashed lines use 4D radion/dilaton EFT (upto two derivatives) to estimate the bounce.

principle, qualitatively in the class described above in figure 3.2, but in this paper we will proceed with our ansatz (3.22).

In an expanding universe the PT completes at a temperature T_n, where the nucleation rate $\Gamma(T_n)$ becomes as large as H^4, that is T_n is found by solving $\Gamma(T_n) = H(T_n)^4$. The solid lines in figure 3.5 show the relation between T_n/T_c and N for fixed $T_c \sim \mathcal{O}(\text{TeV})$ obtained using our 5D ansatz bounce. For comparison, similar curves obtained using 4D radion EFT are shown by the dashed lines in figure 3.5. As shown in figure 3.5, for a fixed λ, both the maximum N and the minimum T for which the PT could happen increase as ϵ gets larger. Also, for a given nucleation temperature T_n, as ϵ increases, completion of PT becomes possible for larger N and thus in better 5D perturbative control.

We emphasize the significance of supercooling on cosmological (dark) matter

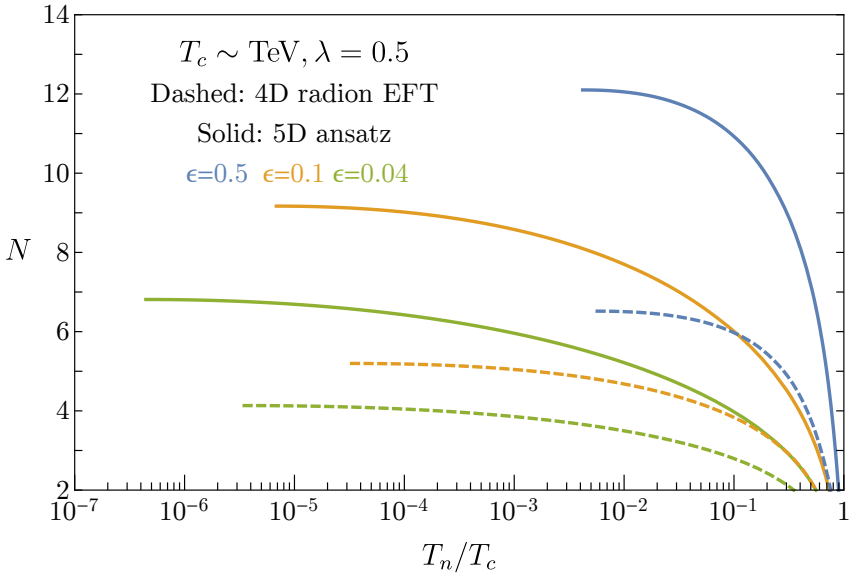

Figure 3.5: Nucleation temperature T_n/T_c (for fixed $T_c \sim \mathcal{O}(\text{TeV})$) as a function of N for various ϵ for fixed $\lambda = 0.5$. The solid lines denote the results using 5D ansatz, while the dashed lines use 4D radion EFT (upto two derivatives) to estimate the bounce. The end point of each curve shows the minimum T_n and maximum N for a given parameter choice.

abundances [41]. For concreteness, we focus on the baryon/lepton asymmetry. We denote this asymmetry before the temperature falls to T_c by Y_{before}, where $Y \equiv \frac{n_B - n_{\bar{B}}}{s}$ where n_B ($n_{\bar{B}}$) is the number density of baryons (antibaryons). Before the PT, as the universe keeps expanding n_B, $n_{\bar{B}}$ and s get diluted $\propto T^3$ and hence Y stays constant. After the PT completes at $T = T_n$, the universes gets reheated to $T \sim T_c$ and unless the PT itself generates an asymmetry, $n_B - n_{\bar{B}}$ does not increase, while s increases to $s \sim T_c^3$ and so after the PT, $Y_{\text{after}} \sim Y_{\text{before}} \left(\frac{T_n}{T_c}\right)^3$. For the observed $Y \sim 10^{-10}$, if $T_n/T_c < \mathcal{O}(10^{-3})$, then even if an $\mathcal{O}(1)$ asymmetry is generated before the PT, it would get diluted to a value below the observed asymmetry by the PT. So such a degree of supercooling, typical of the minimal $\epsilon \sim 1/25$ scenario, is inconsistent with a purely high-scale mechanism for baryogenesis. However, within our two-FP model and by choosing a larger $\epsilon \lesssim 1$, the above dilution is much

smaller, making the PT compatible with baryogenesis above T_c. Of course, it is possible that baryogenesis/dark matter production may take place during or after the transition, see e.g. [64–67], in which case such production does not get overly diluted by supercooling.

In this chapter, we studied the cosmological phase transition of theories with a warped compact extra dimension. We showed how the bubble nucleation rate can be computed using a smooth bounce configuration, within 5D EFT control. This sharpened and completed our analysis of chapter 2, using the dual strongly coupled 4D description. Remarkably this PT generates a stochastic gravitation wave background that can survive until now and be observed by future gravitational wave detectors. In the next chapter, chapter 4, we study the gravitational wave signal produced by the PT.

Chapter 4: Gravitational Wave Signature

In the previous chapters, we showed how to compute the bubble nucleation rate for the cosmological PT of composite Higgs confinement. Using the bubble nucleation rate, we found the region in parameter space for which the PT can complete and the temperature at which this happens. We also discussed some of the phenomenological consequences of this PT for baryonic and dark matter genesis. We now study the direct signature of this PT: the gravitational waves generated during this PT.

When the first order PT, described above, takes place, a stochastic background of gravitational waves (GW) gets generated. Along with the collisions of the bubbles of the confined phase, both the turbulence and the sound waves in the plasma, formed after bubble collisions, can source GW (for reviews see [23,68] and references therein). The properties of GW sourced by the sound waves and turbulence is an active area of research. On the other hand, the contribution from bubble collisions is analytically better understood within the so-called "envelope approximation", but there can be significant corrections such as discussed in [69–73]. In the following we focus on only the contribution due to bubble collisions and for simplicity use the envelope approximation to get a crude sense of the GW signal strength as a

function of our parameters. It is worth keeping in mind that for some parameter space (especially for $T_n \lesssim T_c$ away from the extreme supercooling), the contribution from sound waves and turbulence can dominate over that from bubble collisions.

GW signals from bubble collisions can be characterized by the fractional abundance $\Omega_{\rm GW,b}h^2$ and peak frequency f_p of GW [23]:

$$\Omega_{\rm GW,b}h^2(f) = 1.67\times10^{-5}\left(\frac{H_{\rm PT}}{\beta_{\rm GW}}\right)^2\left(\frac{\kappa_b\alpha}{1+\alpha}\right)^2\left(\frac{100}{g_*}\right)^{1/3}\frac{0.11v_w^3}{0.42+v_w^2}\frac{3.8(f/f_p)^{2.8}}{1+2.8(f/f_p)^{3.8}} \tag{4.1}$$

$$f_p = 1.65\times10^{-4}\ {\rm Hz}\ \frac{0.62}{1.8-0.1v_w+v_w^2}\frac{\beta_{\rm GW}}{H_{\rm PT}}\frac{T_*}{1\ {\rm TeV}}\left(\frac{g_*}{100}\right)^{1/6}, \tag{4.2}$$

where we assume the bubble wall velocity $v_w = 1$; effective degrees of freedom $g_* = 100$; that almost all of the latent heat is transferred to the bubble wall $\kappa_b \approx 1$. α denotes the ratio of the latent heat released in the PT to the energy in the surrounding radiation bath, which is typically $\alpha \gg 1$ for a supercooled PT. Moreover, the duration of phase transition is defined as $1/\beta_{\rm GW}$ and $H_{\rm PT}$ is the Hubble parameter during the PT. T_* is the temperature of the radiation bath right after the PT.

As shown in eq. (4.1), the strength and peak frequency of the gravitational wave signal produced by the phase transition depend strongly on the duration of phase transition, $1/\beta_{\rm GW}$. $\beta_{\rm GW}$ is defined as

$$\frac{\beta_{\rm GW}}{H_{\rm PT}} \equiv -\frac{T}{\Gamma}\frac{d\Gamma}{dT}\Big|_{T_n} \approx -4 + T\frac{dS_b}{dT}\Big|_{T_n}, \tag{4.3}$$

where eq. (3.14) was used.

We now argue, using radion dominance approximation that in the supercooled regime $\beta_{\rm GW}$ is small for small ϵ, as it was pointed out in ref. [41]. In a generic PT, $\frac{dS_{\rm b}}{d\ln T} \sim S_{\rm b} \sim \ln \frac{M_{\rm Pl}}{T_c}$. Remarkably, for small ϵ, $\beta_{\rm GW}$ is suppressed [41] and the GW abundance is enhanced. In order to see this, first note that in the supercooled regime the leading $S_{\rm b}$ in eq. (2.14), is independent of T. The temperature dependence arises from keeping the subleading part of the dilaton potential, eq. (3.9), for small ϕ, in the derivation of eq. (2.14). This effectively results into the replacement in eq. (2.14) of $\lambda_0 \to \lambda_0 \left(1 - \left(\frac{T}{|\lambda_0|^{1/4}\langle\phi\rangle}\right)^{\epsilon}\right)$ as shown in appendix B.

Therefore eq. (4.3) gives

$$\frac{\beta_{\rm GW}}{H_{\rm PT}} \approx -4 + 3\epsilon \left(\frac{T_n}{|\lambda_0|^{1/4}\langle\phi\rangle}\right)^{\epsilon} \ln \frac{M_{\rm Pl}}{T_c}, \tag{4.4}$$

where we have taken $\ln(M_{\rm Pl}/T_c) \gg \ln(T_c/T_n)$. This suppression of $\beta_{\rm GW}$ can allow large enough GW backgrounds so that even the primordial fluctuations contained in it may be observable [52]. As ϵ increases, the PT duration decreases and bubble collision effects become less important, while the less diluted plasma effects become more important.

Here we compute $\beta_{\rm GW}$ using our bounce ansatz and the results are shown in figures 4.1 and 4.2. In figure 4.1 we show the dependence of T_n/T_c and $\beta_{\rm GW}$ on ϵ explicitly with different choices of N and fixed λ. As we can see in (the right panel of) figure 4.1, $\beta_{\rm GW}$ gets smaller as ϵ decreases. In figure 4.2 we show $\beta_{\rm GW}$ as a function of T_n/T_c for fixed λ and different choices of ϵ based on our 5D ansatz. It

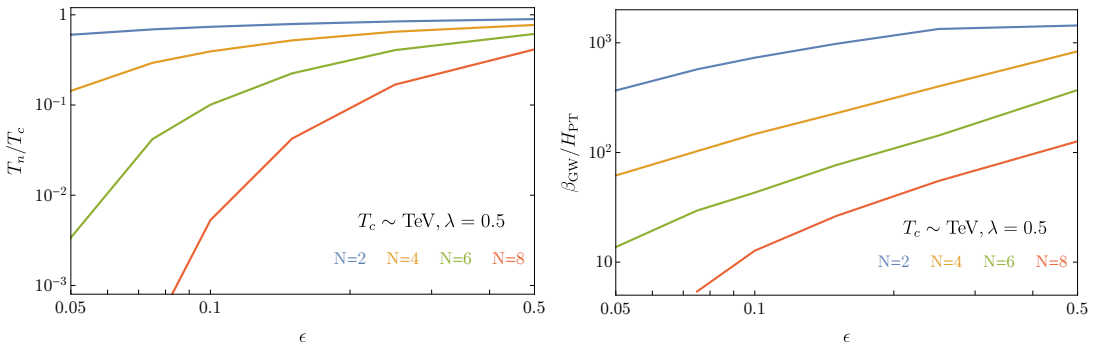

Figure 4.1: Nucleation temperature T_n/T_c (left panel) and $\beta_{\rm GW}/H_{\rm PT}$ (right panel) as a function of ϵ for different choices of N and fixed $\lambda = 0.5$, $T_c \sim \mathcal{O}(\text{TeV})$.

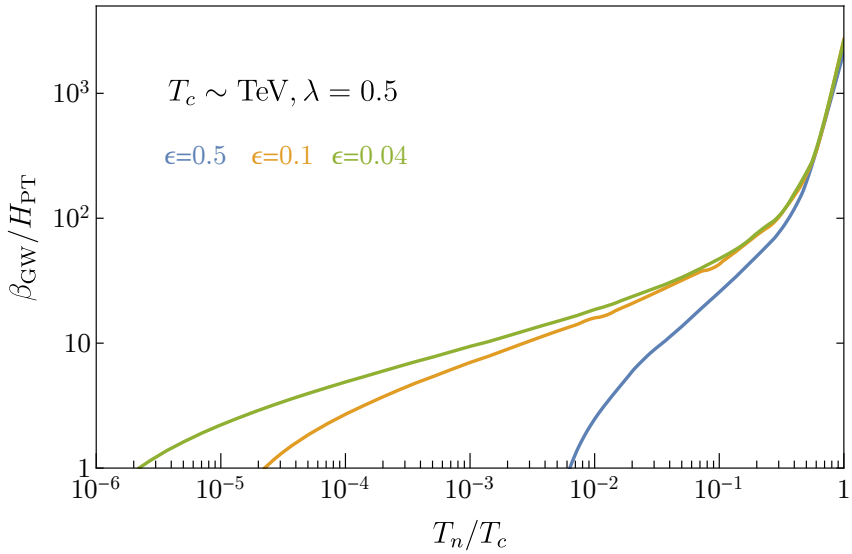

Figure 4.2: $\beta_{\rm GW}/H_{\rm PT}$ as a function of nucleation temperature T_n/T_c for different choices of ϵ and fixed $\lambda = 0.5$, $T_c \sim \mathcal{O}(\text{TeV})$. On each curve, N is varied while ϵ and λ are held fixed.

is clear from figure 4.2 that $\beta_{\rm GW}$ drops as T_n becomes smaller. One can also see from figure 4.2 that to achieve a certain GW signal strength, meaning a given choice of $\beta_{\rm GW}/H_{\rm PT}$, a theory with larger ϵ will have larger T_n/T_c and thus less dilution of primordial matter abundances (see discussion in section 3.5). Moreover, larger ϵ also leads to larger N and better perturbative control.

In figure 4.3 we show the spectrum of the fractional abundance of the GW signal for two choices of β/H and T_c, considering only the more well understood

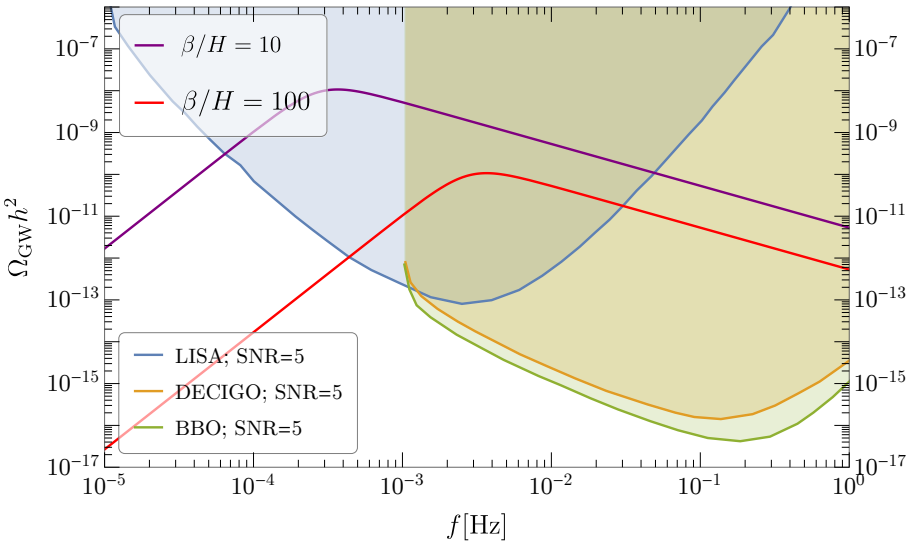

Figure 4.3: The spectrum of GW abundance $\Omega_{\rm GW}h^2$ as a function of GW frequency f from bubble collisions. We choose two sets of benchmark parameters ($\beta/H = 10$, $T_c = $ TeV) and ($\beta/H = 100$, $T_c = $ TeV). The projected sensitivity of LISA, DECIGO and BBO experiments at Signal-to-Noise (SNR) $= 5$ are also included.

contribution of bubble collisions. As mentioned before, the universe will reheat back to temperature around T_c after the PT and thus we take $T_* = T_c$ in figure 4.3. We see that both cases can be observed by LISA, DECIGO and BBO even with this conservative estimate for the gravitational signal. For experimental sensitivity curves, we refer the reader to [74] and references therein. Although the two choices of β/H or T_c above may be realized in the standard RS models, our two-FP model allows larger values of ϵ and thus less dilution of primordial abundances and better perturbative control as mentioned before.

Chapter 5: Conclusions

Composite Higgs models are among the most theoretically motivated candidates for physics beyond the Standard Model (SM). This is because they can address some of the problems of the standard model, by explaining the large observed hierarchies in particle physics. Moreover, they can be probed by current and future high energy collider and low-energy flavor experiments. In these models, the Higgs boson is a composite state of a new strong dynamics at or above the TeV scale, and the early universe can undergo a confinement phase transition (PT) during which Higgs and other composite states are formed. This PT produces gravitational waves that can be detected by future gravitational wave detectors. Therefore, composite Higgs models can result in correlated future collider and gravitational wave signals.

In general the confining dynamics are strongly coupled and non-perturbative, and the PT is difficult to formulate and analyze theoretically. However, in this work we have re-examined such PTs in the context of spontaneous confinement, and shown that the bubble nucleation rate is dominated by relatively simple dilaton dynamics, and that the dominant contribution to the bubble nucleation rate can be computed within the dilaton effective field theory (EFT).

We have also studied theories that have a weakly coupled holographic dual

description of RS1-type, in which we are able to make progress and study the part of the transition that cannot be captured by dilaton EFT. We have shown how *smooth* EFT-controlled 5D bounce configurations can interpolate between the two phases, which in 5D terms are given by a black-brane (dual to deconfined) phase and an IR brane (dual to confined) phase. Our 5D construction goes beyond the conventional ansatz based on 4D radion EFT that is usually employed in the literature. While the usual radion-dominance ansatz can give a correct estimate for the rate of the PT for parametrically small values of model parameters (such as ϵ, λ defined in section 3.1), we find the 5D ansatz does become important for larger values relevant for a realistic PT consistent with observed Planck-Weak hierarchy.

Previous studies have shown that for realistic values of model parameters, consistent with Planck-Weak hierarchy, the Universe often supercools significantly below the critical temperature $\sim$TeV, thereby diluting primordial matter abundances generated before the PT. This makes high-scale mechanisms of (dark) matter genesis potentially incompatible with the minimal Goldberger-Wise radius stabilization mechanism (dual to the composite Higgs theories in the vicinity of a single fixed point).

However, we showed that this conclusion can easily be avoided with the simple generalization of the Goldberger-Wise bulk potential. This is dual to composite Higgs models controlled by separate UV and IR fixed points with separate critical exponents controlling particle hierarchies and the phase transition. Consequently, we have opened up a novel parameter space with only modest cooling, with the associated gravitational waves signal still be readily observable at future detectors,

such as LISA, DECIGO and BBO. In parts of the parameter space, the stochastic gravitational wave background can be sufficiently strong that even primordial anisotropies may be observable [52].

There remain several interesting future directions. While our 5D formulation allows the bounce configuration dominating the transition rate to be semi-classically determined in principle, here we introduced a simple, qualitatively correct, bounce ansatz. We showed this implied a rigorous lower bound on the transition rate in the thin-wall regime, and a very plausible estimate more generally. However, it would be very interesting and important to obtain the true semi-classical bounce configuration. By way of inspiration, in the roughly analogous 6D model of ref. [60] (which however does not address the Hierarchy Problem), a domain wall solution was tractable and can be recast as a semi-classical bounce for the analogous phase transition.

From a more phenomenological perspective, it would also be very interesting to develop baryogenesis mechanisms exploiting the first order nature of the phase transition. Also since our two fixed-point scenario allows for less dilution of pre-existing baryon asymmetry, it is interesting to reconsider baryogenesis mechanisms in composite Higgs models in which asymmetry generation happens before the PT [1]. Alternately, it is interesting to consider warped phase transitions with very different critical temperatures (and thus gravitational wave frequencies) in the context of dark sectors. It is possible that the 5D holographic formulation can be useful to model

[1]For example in refs. [75, 76] high scale leptogenesis has been studied in models which have the structure expected from implementation of standard high-scale seesaw mechanism in the composite Higgs framework.

aspects of the bubble and plasma dynamics relevant for a detailed understanding of the gravitational wave spectrum.

Appendix A: Dominance of $O(3)$ symmetric, time independent bounce

In this appendix, we argue that for small λ_0, the dominant dilaton bounce is $O(3)$ symmetric and independent of $1/T$ periodic Euclidean time as claimed in chapter 2.

Following eqs. (2.2) and (2.5), the generic Euclidean action for the dilaton is given by,

$$S = \frac{N^2}{4\pi|\lambda_0|^{3/4}} \int_0^1 d\tilde{t} \int dx\, x^2 \Big((\partial_x \tilde{\phi})^2 + \frac{1}{|\lambda_0|^{1/2}} (\partial_{\tilde{t}} \tilde{\phi})^2 - \tilde{\phi}^4 \left(1 - \frac{1}{1+\epsilon/4} \left(\frac{T}{|\lambda_0|^{1/4}\langle\phi\rangle} \right)^{\epsilon} \tilde{\phi}^{\epsilon} \right) + 16\pi^2 C \Big) \tag{A.1}$$

where $\tilde{\phi} = |\lambda_0|^{1/4}\phi/T$, $x = |\lambda_0|^{1/4} rT$, $\tilde{t} = tT$. For simplicity, first focus on the case of small T such that $\ln(T_c/T) \gtrsim 1/\epsilon$, where the the potential term proportional to $\tilde{\phi}^{4+\epsilon}$ can be neglected. Due to the periodicity of Euclidean time and the fact that $\tilde{\phi}$ has to change by at least an $\mathcal{O}(1)$ amount in order to interpolate between the deconfined phase ($\tilde{\phi} \approx 0$) and a release point, we get $\partial_{\tilde{t}} \tilde{\phi} \sim \Delta\tilde{\phi}/\Delta\tilde{t} \sim \mathcal{O}(1)$ for a bounce profile $\tilde{\phi}$ that depends on time at the leading order. In this case, for small λ_0, due to the $\frac{1}{|\lambda_0|^{1/2}} (\partial_{\tilde{t}} \tilde{\phi})^2$ term, a time-dependent action is parametrically larger than the time-independent $O(3)$-symmetric bounce eq. (2.14). So the only way to

have a smaller time-dependent bounce action, is to have a bounce that has a leading time-independent part, $\tilde{\phi}_0(x)$, and a subleading time-dependent part, $f(x,t)$:

$$\tilde{\phi}(x,t) = \tilde{\phi}_0(x) + f(x,t), \tag{A.2}$$

where f is of order $|\lambda_0|^{1/4}$ or smaller. The ambiguity of separating $\tilde{\phi}$ into a time dependent and time independent part is removed by requiring that $\int_0^1 d\tilde{t} f = 0$. In this case the action can be expanded in powers of λ_0, which to first nontrivial order in f becomes

$$S \approx \frac{N^2}{4\pi|\lambda_0|^{3/4}} \int_0^1 d\tilde{t} \int dx x^2 \Big((\partial_x \tilde{\phi}_0)^2 - \tilde{\phi_0}^4 + 16\pi^2 C + \frac{1}{|\lambda_0|^{1/2}} (\partial_{\tilde{t}} f)^2 + (\partial_x f)^2 \Big), \tag{A.3}$$

where terms linear in f are not present since they vanish after integrating over t. The quadratic term in f arising from the potential has been dropped since it has a necessarily subdominant contribution to the action for small λ_0. We see that to this order, $\tilde{\phi}_0$ and f have to independently satisfy the equations of motion and a nonzero f has a positive contribution to the action, so that a time-independent bounce solution has a lower action than any such time-dependent configurations/solutions.

In the thin-wall regime, we can parallel the above arguments. In this regime the dominant contribution to the bounce comes from the region where $\phi \sim \langle\phi\rangle \gg T_c$. Thus the effective Lagrangian relevant for a thin-wall bounce can be obtained by

expanding eq. (2.2) around $\langle\phi\rangle$ to get,

$$\mathcal{L}_{\rm eff} = \frac{N^2}{16\pi^2}\left((\partial\phi_s)^2 + 2\epsilon\lambda_0\langle\phi\rangle^2\phi_s^2\right) + \cdots\,, \tag{A.4}$$

where $\phi_s = \phi - \langle\phi\rangle$. Keeping the terms proportional to ϕ_s^3, ϕ_s^4 in the above expansion, will not change the parametric argument that follows. We can recast the above using the rescalings, $\tilde{\phi}_s = (\epsilon|\lambda_0|)^{1/4}\phi_s/T$, $\langle\tilde{\phi}_s\rangle = (\epsilon|\lambda_0|)^{1/4}\langle\phi\rangle/T_c$, $\hat{x} = (\epsilon|\lambda_0|)^{1/4}rT$, $\tilde{t} = tT$, as

$$\mathcal{L}_{\rm eff} \approx \frac{N^2T_c^4}{16\pi^2}\left(\frac{1}{(\epsilon|\lambda_0|^{1/2})}(\partial_{\tilde{t}}\tilde{\phi}_s)^2 + (\partial_{\hat{x}}\tilde{\phi}_s)^2 + 2\langle\tilde{\phi}_s\rangle^2\tilde{\phi}_s^2\right), \tag{A.5}$$

where we have used $T \approx T_c$ which is appropriate for the thin-wall regime. Using the above effective Lagrangian, the Euclidean action can be constructed. Then we can repeat all the arguments given above for the supercooling regime to conclude again that the dominant bounce is time-independent, this time due to the smallness of the quantity $\epsilon\lambda_0$. Even for intermediate T, these arguments can be generalized to show time-independence of the dominant dilaton bounce.

Appendix B: Subleading temperature correction to the bounce action in the supercooled regime

In this section we calculate the subleading correction to $S_{\rm b}$ in the supercooled regime, using which we can find the parameter $\beta_{\rm GW}$ relevant for gravitational waves

as was discussed in chapter 4. There the result of this appendix was used to obtain eq. (4.4). The relevant action can be read off from eq. (A.1) by dropping the time-dependent contribution,

$$S_{\rm b} = \frac{N^2}{4\pi|\lambda_0|^{3/4}} \int dx x^2 \left((\partial_x \tilde{\phi})^2 - \tilde{\phi}^4 \left(1 - \frac{1}{1+\epsilon/4} \left(\frac{T}{|\lambda_0|^{1/4}\langle\phi\rangle} \right)^{\epsilon} \tilde{\phi}^{\epsilon} \right) + 16\pi^2 C \right). \tag{B.1}$$

We will expand in $\left(\frac{T}{|\lambda_0|^{1/4}\langle\phi\rangle}\right)^{\epsilon}$ by treating the term in the potential proportional to $\tilde{\phi}^{4+\epsilon}$ as a perturbation, and obtain the leading temperature correction to $S_{\rm b}$ by first solving the "zeroth-order" bounce equation in the absence of the $\tilde{\phi}^{4+\epsilon}$ term. Let us denote such a bounce solution as $\tilde{\phi}_0(x)$ and the corresponding zeroth-order bounce action as $S_{\rm b}^{(0)}$. The leading correction to $S_{\rm b}^{(0)}$ is then given by

$$\Delta S_{\rm b} = \frac{N^2}{4\pi|\lambda_0|^{3/4}} \frac{1}{1+\epsilon/4} \left(\frac{T}{|\lambda_0|^{1/4}\langle\phi\rangle} \right)^{\epsilon} \int dx x^2 \tilde{\phi}_0^{4+\epsilon}. \tag{B.2}$$

Note that even though the solution $\tilde{\phi}$ is corrected by the perturbation, the change of the action due to this correction vanishes to first order since the first variation of the action vanishes when evaluated on the solution of equation of motion. Then, for small ϵ, we can approximate the above correction as,

$$\Delta S_b \approx \frac{N^2}{4\pi|\lambda_0|^{3/4}} \left(\frac{T}{|\lambda_0|^{1/4}\langle\phi\rangle} \right)^{\epsilon} \int dx x^2 \tilde{\phi}_0^4. \tag{B.3}$$

This implies the temperature dependent bounce action can be approximated as,

$$S_{\rm b} \approx \frac{N^2}{4\pi|\lambda_0|^{3/4}} \int dx x^2 \left((\partial_x \tilde{\phi}_0)^2 - \tilde{\phi}_0^4 \left(1 - \frac{1}{1+\epsilon/4} \left(\frac{T}{|\lambda_0|^{1/4}\langle\phi\rangle} \right)^\epsilon \right) + 16\pi^2 C \right) \quad \text{(B.4)}$$

$$\approx \frac{N^2}{4\pi T} \int dr r^2 \left(\left(\frac{d\phi}{dr} \right)^2 + \lambda_0 \left(1 - \left(\frac{T}{|\lambda_0|^{1/4}\langle\phi\rangle} \right)^\epsilon \right) \phi^4 + 16\pi^2 C T^4 \right), \quad \text{(B.5)}$$

where in the second line we have re-expressed the action in terms of ϕ and r. Therefore including this subleading temperature correction is equivalent to a corresponding change in the dilaton quartic coupling,

$$\lambda_0 \to \lambda_0 \left(1 - \left(\frac{T}{|\lambda_0|^{1/4}\langle\phi\rangle} \right)^\epsilon \right) \quad \text{(B.6)}$$

in eq. (2.13). Thus to first order in $\left(\frac{T}{|\lambda_0|^{1/4}\langle\phi\rangle} \right)^\epsilon$ and for small ϵ we have using eq. (2.14),

$$S_{\rm b} \approx S_{\rm b}^{(0)} \left(1 + \frac{3}{4} \left(\frac{T}{|\lambda_0|^{1/4}\langle\phi\rangle} \right)^\epsilon \right), \quad \text{(B.7)}$$

which when used in eq. (4.3) gives eq. (4.4).

Appendix C: Radion potential for the 5D model of the two fixed points

In this appendix, we complete the derivation of an analytic approximation to the radion potential, eq. (3.36), in our two-FP scenario introduced in section 3.4.

As discussed in section 3.4, we consider the following polynomial potential for the Goldberger-Wise field, eq. (3.31):

$$V(\chi) = \frac{1}{2}m'^2\chi^2 + \frac{1}{6}\eta\,\chi^3 + \frac{1}{24}g\,\chi^4 \tag{C.1}$$

where we assume the following signs for the coefficients in the potential: $m'^2 < 0, \eta < 0$, and $g > 0$. The EoM for χ is

$$\frac{d^2}{d\sigma^2}\chi - 4\frac{d}{d\sigma}\chi - V'(\chi) = 0, \tag{C.2}$$

where σ is the extra dimensional coordinate with the range $0 < \sigma < L$ and differentiation with respect to σ will be denoted by a dot. We consider the following boundary conditions, as in eq. (3.7) for χ,

$$\chi(\sigma = 0) = v, \tag{C.3}$$

$$\dot{\chi}(\sigma = L) = \alpha, \tag{C.4}$$

which can be obtained from boundary potential terms for the GW field,

$$S_\chi^{\rm UV} = -\int d^4x\ \kappa\sqrt{-\gamma_{\rm UV}}\left(\chi^2 - v^2\right)^2, \tag{C.5}$$

$$S_\chi^{\rm IR} = \int d^4x\ \sqrt{-\gamma_{\rm IR}}\ \alpha\chi, \tag{C.6}$$

where $S_\chi^{\rm UV}$ and $S_\chi^{\rm IR}$ denote the UV and IR brane terms respectively. To impose the UV boundary condition, $\chi(\sigma = 0) = v$, one needs to take the limit of large κ. In

this limit the only effect of this term is setting the boundary condition and does not have any extra contribution to the radion potential. The $S_\chi^{\rm IR}$ term, on the other hand, will contribute to the radion potential.

As mentioned in section 3.4, the above potential in eq. (C.1) has two extrema[1] at

$$\chi = 0 \text{ and } \chi = \chi_* = \frac{3}{g}\left(-\frac{\eta}{2} + \sqrt{\frac{\eta^2}{4} - \frac{2gm'^2}{3}}\right), \tag{C.7}$$

corresponding to two constant-χ solutions of EoM. To compute the radion potential analytically, we approximate the Goldberger-Wise bulk potential by a piecewise-quadratic potential given by

$$\tilde{V}_\chi(\chi) = \begin{cases} \frac{1}{2}m'^2\chi^2 & \chi \le \chi_{\rm m} \\ \\ \frac{1}{2}m^2(\chi-\chi_*)^2 - C & \chi > \chi_{\rm m} \end{cases}, \tag{C.8}$$

where $m^2 \equiv V_\chi''(\chi_*) = -2m'^2 - \eta\chi_*/2$ and we have matched the two approximations at $\chi_{\rm m} = (-\eta + \sqrt{\eta^2 - 2gm'^2})/g$ corresponding to the inflection point of the potential in eq. (C.1). The constant $C = \frac{1}{2}m^2(\chi_{\rm m} - \chi_*)^2 - \frac{1}{2}m'^2\chi_{\rm m}^2$ ensures the continuity of $\tilde{V}_\chi(\chi)$. We are interested in the case of $|m'^2| \ll m^2$, using which we get $\chi_{\rm m} \approx \frac{2}{3}\chi_*$ and $C \approx \frac{1}{18}m^2\chi_*^2$.

We choose v in the range $0 < v < \chi_*$, and close to $\chi = 0$. With this choice, for small enough L, the field value is always smaller than $\chi_{\rm m}$ and thus $\tilde{V}_\chi(\chi)$ in

[1]The potential of eq. (C.1) has another extremum in $\chi < 0$, but that is not important for the solutions for χ that we consider here, as we choose the UV boundary value v to be on the range $0 < v < \chi_*$.

eq. (C.8) reduces to the standard quadratic potential. In this case, the standard Goldberger-Wise solution applies [35]:

$$\chi(\sigma) \approx v e^{\epsilon'\sigma} + \frac{\alpha}{4} e^{(4-\epsilon')(\sigma-L)} \qquad (\text{for } L < L_{\rm m}), \tag{C.9}$$

where $\epsilon' = 2 - \sqrt{4+m'^2}$ and we have dropped terms that are higher order in ϵ' and e^{-L}. We define $L_{\rm m}$ as the special value of L that satisfies:

$$\chi(L)|_{L=L_{\rm m}} = \chi_{\rm m} \quad \to \quad L_{\rm m} \approx \frac{1}{\epsilon'} \ln\left(\frac{\chi_{\rm m} - \alpha/4}{v}\right). \tag{C.10}$$

It is easy to see from eq. (C.9) that in the region $L < L_{\rm m}$, the field profile $\chi(\sigma)$ always stays smaller than $\chi_{\rm m}$ and thus it was self-consistent to use eq. (C.9).

For larger values of L, i.e. for $L > L_{\rm m}$, the solution has the form

$$\chi(\sigma) = \begin{cases} A_1 e^{\epsilon'\sigma} + A_2 e^{(4-\epsilon')\sigma} & \sigma < \sigma_{\rm m} \\ B_1 e^{-\epsilon(\sigma-\sigma_{\rm m})} + B_2 e^{(4+\epsilon)(\sigma-\sigma_{\rm m})} + \chi_* & \sigma > \sigma_{\rm m} \end{cases} \tag{C.11}$$

in which $\sigma_{\rm m}$ is defined as $\chi(\sigma_{\rm m}) = \chi_{\rm m}$ and $\epsilon = -2 + \sqrt{4+m^2}$.[2] In the expression above A_i, B_i, $\sigma_{\rm m}$ are independent of σ, but are in general L-dependent. In addition to the two boundary conditions, there are three other conditions that we have to impose to solve for the five unknowns $A_{1,2}$, $B_{1,2}$ and $\sigma_{\rm m}$. These conditions are continuity of χ and $\dot{\chi}$ at $\sigma_{\rm m}$, implied by continuity of $V(\chi)$(or finiteness of $V'(\chi)$) and the EoM for χ, and that the field value is equal to $\chi_{\rm m}$ at $\sigma_{\rm m}$. So we need to

[2] We choose to work with positive ϵ and ϵ' and thus there is a sign difference in their expressions.

solve the following set of equations:

$$\begin{cases} A_1 + A_2 = v \\ A_1 e^{\epsilon' \sigma_{\rm m}} + A_2 e^{(4-\epsilon')\sigma_{\rm m}} = \chi_{\rm m} \\ \epsilon' A_1 e^{\epsilon' \sigma_{\rm m}} + (4-\epsilon') A_2 e^{(4-\epsilon')\sigma_{\rm m}} = -\epsilon B_1 + (4+\epsilon) B_2 \\ B_1 + B_2 = \chi_{\rm m} - \chi_* \\ -\epsilon B_1 e^{-\epsilon(L-\sigma_{\rm m})} + (4+\epsilon) B_2 e^{(4+\epsilon)(L-\sigma_{\rm m})} = \alpha \end{cases} \tag{C.12}$$

In terms of $\sigma_{\rm m}$ the first two and last two equations can be solved separately:

$$\begin{cases} A_1 \approx v - \chi_{\rm m} e^{-(4-\epsilon')\sigma_{\rm m}} \\ A_2 \approx \chi_{\rm m} e^{-(4-\epsilon')\sigma_{\rm m}} - v e^{-(4-2\epsilon')\sigma_{\rm m}} \\ B_1 = \frac{(4+\epsilon)(\chi_{\rm m}-\chi_*)e^{(4+\epsilon)(L-\sigma_{\rm m})} - \alpha}{(4+\epsilon)e^{(4+\epsilon)(L-\sigma_{\rm m})} + \epsilon\, e^{-\epsilon(L-\sigma_{\rm m})}} \approx (\chi_{\rm m} - \chi_*) - \frac{\alpha}{4+\epsilon} e^{-(4+\epsilon)(L-\sigma_{\rm m})} \\ B_2 = \frac{\alpha - \epsilon(\chi_* - \chi_{\rm m})\, e^{-\epsilon(L-\sigma_{\rm m})}}{(4+\epsilon)e^{(4+\epsilon)(L-\sigma_{\rm m})} - \epsilon\, e^{-\epsilon(L-\sigma_{\rm m})}} \approx \frac{\alpha}{4+\epsilon} e^{-(4+\epsilon)(L-\sigma_{\rm m})} - \frac{\epsilon}{4+\epsilon}(\chi_* - \chi_{\rm m}) e^{-(4+2\epsilon)(L-\sigma_{\rm m})} \end{cases} \tag{C.13}$$

Now putting these into the third equation of eqs. (C.12), we find an equation for $\sigma_{\rm m}$:

$$-(4-2\epsilon')v e^{\epsilon' \sigma_{\rm m}} + (4-\epsilon')\chi_{\rm m} \approx \epsilon(\chi_* - \chi_{\rm m}) + \left(\alpha - \epsilon(\chi_* - \chi_{\rm m}) e^{-\epsilon(L-\sigma_{\rm m})}\right) e^{-(4+\epsilon)(L-\sigma_{\rm m})}. \tag{C.14}$$

The right-hand-side of this equation becomes small quickly as $L - \sigma_{\rm m}$ increases,

making $e^{\epsilon'\sigma_{\rm m}}$ weakly dependent on L. Expanding in ϵ' and $e^{-(L-\sigma_{\rm m})}$ we get

$$e^{\epsilon'\sigma_{\rm m}} \approx \frac{\chi_{\rm m} - \frac{\epsilon}{4}(\chi_* - \chi_{\rm m}) + \frac{\epsilon'}{4}\chi_{\rm m}}{v} - \frac{\alpha}{4v}\left(\frac{\chi_{\rm m} - \frac{\epsilon}{4}(\chi_* - \chi_{\rm m}) + \frac{\epsilon'}{4}\chi_{\rm m}}{v}\right)^{\frac{4+\epsilon}{\epsilon'}} \phi^{4+\epsilon}. \quad \text{(C.15)}$$

We now move on to calculate the radion potential. As mentioned in section 3.1, radion action is obtained by promoting e^{-L} to $\phi(x)$ in $S_{\rm 5D}$ (eq. (3.1)). The dominant contribution to 4D radion potential $V_{\rm rad}(\phi)$ comes from S_χ (eq. (3.6)) after integrating over the 5th dimension. For $\phi > \phi_{\rm m} \equiv e^{-L_{\rm m}}$, the Goldberger-wise scalar $\chi(\sigma)$ has the standard form eq. (C.9) and thus the radion potential is the same as eq. (3.9). For $\phi < \phi_{\rm m}$, Goldberger-wise scalar $\chi(\sigma)$ has the form in eq. (C.11) given our piecewise-potential approximation in eq. (C.8). Similar to case of free Goldberger-Wise field, we can use the EoM in the bulk and then integrate by parts to get the radion potential in terms of only the boundary terms:

$$V_{\rm rad}(L) \supset \left[\frac{1}{2}e^{-4\sigma}\chi\dot{\chi}\right]_{\sigma=0}^{\sigma_{\rm m}} + \left[\frac{1}{2}e^{-4\sigma}(\chi - \chi_*)\dot{\chi}\right]_{\sigma=\sigma_{\rm m}}^{L} - e^{-4L}\alpha\chi(L) + \frac{C}{4}\left[e^{-4\sigma}\right]_{\sigma=\sigma_{\rm m}}^{L}, \quad \text{(C.16)}$$

which in terms of ϕ and the coefficients $A_{1,2}$ and $B_{1,2}$ becomes

$$\begin{aligned} V_{\rm rad}(\phi) \supset & -\tfrac{1}{2}\alpha\phi^4\left(2\chi_* + B_1\left(e^{\sigma_{\rm m}}\phi\right)^{\epsilon} + B_2\left(e^{\sigma_{\rm m}}\phi\right)^{-(4+\epsilon)}\right) + \tfrac{1}{2}\chi_* e^{-4\sigma_{\rm m}}\left(-\epsilon B_1 + (4+\epsilon)B_2\right) \\ & -\tfrac{1}{2}v\left(\epsilon' A_1 + (4-\epsilon')A_2\right) - \tfrac{C}{4}(e^{-4\sigma_{\rm m}} - e^{-4L}). \end{aligned} \quad \text{(C.17)}$$

Substituting the coefficients in eq. (C.17) and including the IR brane tension de-

tuning and dropping the constant terms, we obtain the following radion potential keeping the leading order in ϵ and ϵ':

$$V_{\rm rad}(\phi) \approx \begin{cases} \tau\phi^4 - \alpha v \phi^{4-\epsilon'} & \phi > \phi_{\rm m} \\ (\tau - \alpha\chi_*)\phi^4 + \alpha(\chi_* - \chi_{\rm m}) \left(\frac{\chi_{\rm m} - \frac{\epsilon}{4}(\chi_* - \chi_{\rm m})}{v}\right)^{\epsilon/\epsilon'} \phi^{4+\epsilon} & \phi \ll \phi_{\rm m} \end{cases}, \quad \text{(C.18)}$$

where $\tau \equiv \tau_{\rm IR} + 12M_5^3 - \alpha^2/8$ and $\tau_{\rm IR}$ is allowed to be detuned away from the RS value $-12M_5^3$.

We can choose $\tau > 0$ and $\tau' \equiv \tau - \alpha\chi_* < 0$ while all other parameters in eq. (C.18) are positive. For this choice of parameters, the above potential in eq. (C.18) has only one minimum which is located in the $\phi < \phi_{\rm m}$ range:

$$\langle\phi\rangle \sim \left(\frac{v}{\chi_{\rm m}(1 - \epsilon/8)}\right)^{1/\epsilon'} \left(\frac{-2\tau'}{\alpha\chi_{\rm m}}\right)^{1/\epsilon}, \quad \text{(C.19)}$$

where we have used $\chi_{\rm m} \approx \frac{2}{3}\chi_*$ to simplify the expression. This completes the derivation of eqs (3.36) and (3.37), mentioned in section 3.4.

Bibliography

[1] Kaustubh Agashe, Peizhi Du, Majid Ekhterachian, Soubhik Kumar, and Raman Sundrum. Cosmological Phase Transition of Spontaneous Confinement. *JHEP*, 05:086, 2020.

[2] Kaustubh Agashe, Peizhi Du, Majid Ekhterachian, Soubhik Kumar, and Raman Sundrum. Phase Transitions from the Fifth Dimension. *JHEP*, 02:051, 2021.

[3] Paolo Creminelli, Alberto Nicolis, and Riccardo Rattazzi. Holography and the electroweak phase transition. *JHEP*, 03:051, 2002.

[4] Georges Aad et al. Observation of a new particle in the search for the Standard Model Higgs boson with the ATLAS detector at the LHC. *Phys. Lett.*, B716:1–29, 2012.

[5] Serguei Chatrchyan et al. Observation of a New Boson at a Mass of 125 GeV with the CMS Experiment at the LHC. *Phys. Lett.*, B716:30–61, 2012.

[6] Stephen P. Martin. A Supersymmetry primer. *Adv. Ser. Direct. High Energy Phys.*, 18:1–98, 1998.

[7] Brando Bellazzini, Csaba Csáki, and Javi Serra. Composite Higgses. *Eur. Phys. J.*, C74(5):2766, 2014.

[8] Giuliano Panico and Andrea Wulzer. The Composite Nambu-Goldstone Higgs. *Lect. Notes Phys.*, 913:pp.1–316, 2016.

[9] Sidney Coleman. *Aspects of Symmetry*. Cambridge University Press, Cambridge, U.K., 1985.

[10] Juan Martin Maldacena. The Large N limit of superconformal field theories and supergravity. *Int. J. Theor. Phys.*, 38:1113–1133, 1999. [Adv. Theor. Math. Phys.2,231(1998)].

[11] Edward Witten. Anti-de Sitter space and holography. *Adv. Theor. Math. Phys.*, 2:253–291, 1998.

[12] Ofer Aharony, Steven S. Gubser, Juan Martin Maldacena, Hirosi Ooguri, and Yaron Oz. Large N field theories, string theory and gravity. *Phys. Rept.*, 323:183–386, 2000.

[13] Lisa Randall and Raman Sundrum. A Large mass hierarchy from a small extra dimension. *Phys. Rev. Lett.*, 83:3370–3373, 1999.

[14] Lisa Randall and Raman Sundrum. An Alternative to compactification. *Phys. Rev. Lett.*, 83:4690–4693, 1999.

[15] Nima Arkani-Hamed, Massimo Porrati, and Lisa Randall. Holography and phenomenology. *JHEP*, 08:017, 2001.

[16] R. Rattazzi and A. Zaffaroni. Comments on the holographic picture of the Randall-Sundrum model. *JHEP*, 04:021, 2001.

[17] Hooman Davoudiasl, Shrihari Gopalakrishna, Eduardo Ponton, and Jose Santiago. Warped 5-Dimensional Models: Phenomenological Status and Experimental Prospects. *New J. Phys.*, 12:075011, 2010.

[18] Tony Gherghetta. A Holographic View of Beyond the Standard Model Physics. 2011.

[19] Arthur Kosowsky, Michael S. Turner, and Richard Watkins. Gravitational radiation from colliding vacuum bubbles. *Phys. Rev.*, D45:4514–4535, 1992.

[20] Arthur Kosowsky and Michael S. Turner. Gravitational radiation from colliding vacuum bubbles: envelope approximation to many bubble collisions. *Phys. Rev.*, D47:4372–4391, 1993.

[21] Arthur Kosowsky, Michael S. Turner, and Richard Watkins. Gravitational waves from first order cosmological phase transitions. *Phys. Rev. Lett.*, 69:2026–2029, 1992.

[22] Marc Kamionkowski, Arthur Kosowsky, and Michael S. Turner. Gravitational radiation from first order phase transitions. *Phys. Rev.*, D49:2837–2851, 1994.

[23] Chiara Caprini et al. Science with the space-based interferometer eLISA. II: Gravitational waves from cosmological phase transitions. *JCAP*, 1604(04):001, 2016.

[24] Mariano Quiros. Finite temperature field theory and phase transitions.

[25] Pau Amaro-Seoane et al. Laser Interferometer Space Antenna. 2017.

[26] G. M. Harry, P. Fritschel, D. A. Shaddock, W. Folkner, and E. S. Phinney. Laser interferometry for the big bang observer. *Class. Quant. Grav.*, 23:4887–4894, 2006. [Erratum: Class. Quant. Grav.23,7361(2006)].

[27] Peter W. Graham, Jason M. Hogan, Mark A. Kasevich, Surjeet Rajendran, and Roger W. Romani. Mid-band gravitational wave detection with precision atomic sensors. 2017.

[28] Seiji Kawamura et al. The Japanese space gravitational wave antenna: DECIGO. *Class. Quant. Grav.*, 28:094011, 2011.

[29] Xuefei Gong et al. Descope of the ALIA mission. *J. Phys. Conf. Ser.*, 610(1):012011, 2015.

[30] Abdus Salam and J. Strathdee. Nonlinear realizations. ii. conformal symmetry. *Phys. Rev.*, 184:1760–1768, Aug 1969.

[31] Walter D. Goldberger and Mark B. Wise. Modulus stabilization with bulk fields. *Phys. Rev. Lett.*, 83:4922–4925, 1999.

[32] Walter D. Goldberger, Benjamin Grinstein, and Witold Skiba. Distinguishing the Higgs boson from the dilaton at the Large Hadron Collider. *Phys. Rev. Lett.*, 100:111802, 2008.

[33] Zackaria Chacko and Rashmish K. Mishra. Effective Theory of a Light Dilaton. *Phys. Rev.*, D87(11):115006, 2013.

[34] Brando Bellazzini, Csaba Csaki, Jay Hubisz, Javi Serra, and John Terning. A Higgslike Dilaton. *Eur. Phys. J.*, C73(2):2333, 2013.

[35] Zackaria Chacko, Rashmish K. Mishra, and Daniel Stolarski. Dynamics of a Stabilized Radion and Duality. *JHEP*, 09:121, 2013.

[36] Francesco Coradeschi, Paolo Lodone, Duccio Pappadopulo, Riccardo Rattazzi, and Lorenzo Vitale. A naturally light dilaton. *JHEP*, 11:057, 2013.

[37] Zackaria Chacko, Rashmish K. Mishra, Daniel Stolarski, and Christopher B. Verhaaren. Interactions of a Stabilized Radion and Duality. *Phys. Rev. D*, 92(5):056004, 2015.

[38] Lisa Randall and Geraldine Servant. Gravitational waves from warped spacetime. *JHEP*, 05:054, 2007.

[39] Jared Kaplan, Philip C. Schuster, and Natalia Toro. Avoiding an Empty Universe in RS I Models and Large-N Gauge Theories. 2006.

[40] Germano Nardini, Mariano Quiros, and Andrea Wulzer. A Confining Strong First-Order Electroweak Phase Transition. *JHEP*, 09:077, 2007.

[41] Thomas Konstandin and Geraldine Servant. Cosmological Consequences of Nearly Conformal Dynamics at the TeV scale. *JCAP*, 1112:009, 2011.

[42] Benedict von Harling and Geraldine Servant. QCD-induced Electroweak Phase Transition. *JHEP*, 01:159, 2018.

[43] Sebastian Bruggisser, Benedict Von Harling, Oleksii Matsedonskyi, and Géraldine Servant. Baryon Asymmetry from a Composite Higgs Boson. *Phys. Rev. Lett.*, 121(13):131801, 2018.

[44] Sebastian Bruggisser, Benedict Von Harling, Oleksii Matsedonskyi, and Géraldine Servant. Electroweak Phase Transition and Baryogenesis in Composite Higgs Models. *JHEP*, 12:099, 2018.

[45] Pietro Baratella, Alex Pomarol, and Fabrizio Rompineve. The Supercooled Universe. *JHEP*, 03:100, 2019.

[46] Babiker Hassanain, John March-Russell, and Martin Schvellinger. Warped Deformed Throats have Faster (Electroweak) Phase Transitions. *JHEP*, 10:089, 2007.

[47] Thomas Konstandin, Germano Nardini, and Mariano Quiros. Gravitational Backreaction Effects on the Holographic Phase Transition. *Phys. Rev.*, D82:083513, 2010.

[48] Barry M. Dillon, Basem Kamal El-Menoufi, Stephan J. Huber, and Jonathan P. Manuel. Rapid holographic phase transition with brane-localized curvature. *Phys. Rev.*, D98(8):086005, 2018.

[49] Don Bunk, Jay Hubisz, and Bithika Jain. A Perturbative RS I Cosmological Phase Transition. *Eur. Phys. J.*, C78(1):78, 2018.

[50] Eugenio Megias, Germano Nardini, and Mariano Quiros. Cosmological Phase Transitions in Warped Space: Gravitational Waves and Collider Signatures. *JHEP*, 09:095, 2018.

[51] Kohei Fujikura, Yuichiro Nakai, and Masaki Yamada. A more attractive scheme for radion stabilization and supercooled phase transition. *JHEP*, 02:111, 2020.

[52] Michael Geller, Anson Hook, Raman Sundrum, and Yuhsin Tsai. Primordial Anisotropies in the Gravitational Wave Background from Cosmological Phase Transitions. *Phys. Rev. Lett.*, 121(20):201303, 2018.

[53] Pedro Schwaller. Gravitational Waves from a Dark Phase Transition. *Phys. Rev. Lett.*, 115(18):181101, 2015.

[54] Aneesh V. Manohar. Large N QCD.

[55] Sidney R. Coleman. The Fate of the False Vacuum. 1. Semiclassical Theory. *Phys. Rev.*, D15:2929–2936, 1977. [Erratum: Phys. Rev.D16,1248(1977)].

[56] Andrei D. Linde. Decay of the False Vacuum at Finite Temperature. *Nucl. Phys.*, B216:421, 1983. [Erratum: Nucl. Phys.B223,544(1983)].

[57] S.W. Hawking and Don N. Page. Thermodynamics of Black Holes in anti-De Sitter Space. *Commun. Math. Phys.*, 87:577, 1983.

[58] Eugenio Megias, Germano Nardini, and Mariano Quiros. Gravitational Imprints from Heavy Kaluza-Klein Resonances. *Phys. Rev. D*, 102(5):055004, 2020.

[59] Francesco Bigazzi, Alessio Caddeo, Aldo L. Cotrone, and Angel Paredes. Fate of false vacua in holographic first-order phase transitions. 8 2020.

[60] Ofer Aharony, Shiraz Minwalla, and Toby Wiseman. Plasma-balls in large N gauge theories and localized black holes. *Class. Quant. Grav.*, 23:2171–2210, 2006.

[61] James W. York. Role of conformal three-geometry in the dynamics of gravitation. *Phys. Rev. Lett.*, 28:1082–1085, Apr 1972.

[62] G. W. Gibbons and S. W. Hawking. Action integrals and partition functions in quantum gravity. *Phys. Rev. D*, 15:2752–2756, May 1977.

[63] Ivo Savonije and Erik P. Verlinde. CFT and entropy on the brane. *Phys. Lett. B*, 507:305–311, 2001.

[64] Thomas Konstandin and Geraldine Servant. Natural Cold Baryogenesis from Strongly Interacting Electroweak Symmetry Breaking. *JCAP*, 07:024, 2011.

[65] Geraldine Servant. Baryogenesis from Strong CP Violation and the QCD Axion. *Phys. Rev. Lett.*, 113(17):171803, 2014.

[66] Oleksii Matsedonskyi and Geraldine Servant. High-Temperature Electroweak Symmetry Non-Restoration from New Fermions and Implications for Baryogenesis. *JHEP*, 09:012, 2020.

[67] Iason Baldes, Yann Gouttenoire, and Filippo Sala. String Fragmentation in Supercooled Confinement and implications for Dark Matter. 7 2020.

[68] Chiara Caprini et al. Detecting gravitational waves from cosmological phase transitions with LISA: an update. *JCAP*, 03:024, 2020.

[69] Ryusuke Jinno and Masahiro Takimoto. Gravitational waves from bubble dynamics: Beyond the Envelope. *JCAP*, 01:060, 2019.

[70] Thomas Konstandin. Gravitational radiation from a bulk flow model. *JCAP*, 03:047, 2018.

[71] Marek Lewicki and Ville Vaskonen. Gravitational wave spectra from strongly supercooled phase transitions. 7 2020.

[72] Stefan Höche, Jonathan Kozaczuk, Andrew J. Long, Jessica Turner, and Yikun Wang. Towards an all-orders calculation of the electroweak bubble wall velocity. 7 2020.

[73] John Ellis, Marek Lewicki, and Ville Vaskonen. Updated predictions for gravitational waves produced in a strongly supercooled phase transition. 7 2020.

[74] Kai Schmitz. New Sensitivity Curves for Gravitational-Wave Experiments. 2 2020.

[75] Kaustubh Agashe, Peizhi Du, Majid Ekhterachian, Chee Sheng Fong, Sungwoo Hong, and Luca Vecchi. Hybrid seesaw leptogenesis and TeV singlets. *Phys. Lett. B*, 785:489–497, 2018.

[76] Kaustubh Agashe, Peizhi Du, Majid Ekhterachian, Chee Sheng Fong, Sungwoo Hong, and Luca Vecchi. Natural Seesaw and Leptogenesis from Hybrid of High-Scale Type I and TeV-Scale Inverse. *JHEP*, 04:029, 2019.